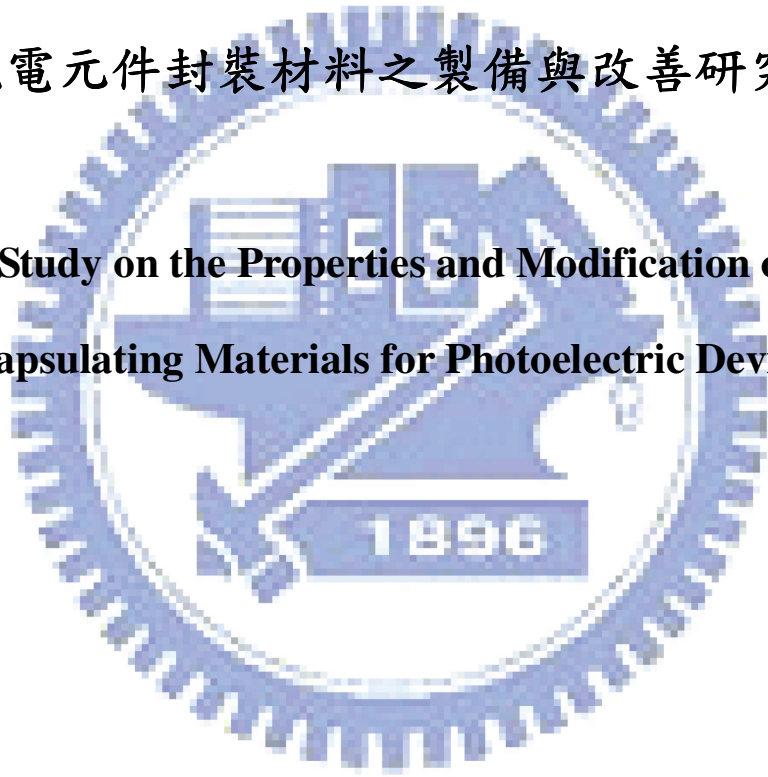# 國立交通大學

材料科學與工程學系

博士論文

光電元件封裝材料之製備與改善研究

A Study on the Properties and Modification of

Encapsulating Materials for Photoelectric Devices

研 究 生：陳建明

指導教授：謝宗雍 博士

中華民國九十八年六月

光電元件封裝材料之製備與改善研究

A Study on the Properties and Modification of
Encapsulating Materials for Photoelectric Devices

研 究 生：陳建明　　　　　　　Student： Chen-Ming Chen

指導教授：謝宗雍 博士　　　　　Advisor： Dr. Tsung-Eong Hsieh

國立交通大學

材料科學與工程學系

博士論文

A Thesis

Submitted to Department of Materials Science and Engineering

College of Engineering

National Chiao-Tung University

in partial Fulfillment of the Requirements

for the Degree of

Doctor of Philosophy

in

Materials Science and Engineering

July 2009

Hsinchu, Taiwan, Republic of China

中華民國九十八年六月

光電元件封裝材料之性質與改善研究

學生姓名：陳建明　　　　　　　　　　　指導教授：謝宗雍 博士

國立交通大學　材料科學與工程學系

摘　　要

本論文研究各種紫外光硬化高分子複合膠材（聚氨基甲酸脂-丙烯酸脂/氧化矽（PU-acrylate/Silica = 90 wt.%/10 wt.%）、矽氧樹脂 - 丙烯酸脂 /氧化 鋁（Silicone-acrylate/Alumina = 90 wt.%/10 wt.%）環氧樹脂-丙烯酸脂/氧化矽/Invar 合金（Epoxy-acrylate/Silica/Invar= 35 wt.%/50 wt.%/15 wt.%）之製備，並將其應用至有機發光二極體（Organic Light-emitting Devices，OLEDs）、有機太陽能電池（Organic Solar Cells，OSCs）與發光二極體（Light-emitting Diodes，LEDs）之封裝。OLED 之封裝部分之研究發現藉由調控氟化鋰（Lithium Fluoride，LiF）的厚度並以自製的封裝膠進行封裝能阻擋空氣中的水氣與氧氣進入 OLEDs 中，其可成功地提升 OLED 的壽命達未封裝的 18 倍。OLED 的研究中亦建構了低起始電壓（Turn-on Voltage = 3 V）　高亮度（於 9 V 驅動下可達 4850 cd/m^2）　顏色/亮度可調之 OLEDs，其結構為 ITO Glass/naphthyl phenyl benzidine (NPB; 80 nm)/4,4'-bis (diphenylvinylenyl)-biphenyl (ADS082BE; 35 nm)/1,3-bis [2-(2,2'-bipyridine-6-yl)-1,3,4-oxadiazo-5-yl] benzene (Bpy-OXD; 20 nm)/

tris-[8-hydroxy-quinoline]aluminum (Alq$_3$; 50 nm)/(LiF; 3 nm)/Aluminum (Al; 80 nm)，其電致變色性質（光色、發光強度等）可藉由調整 NPB/ADS082BE/Bpy-OXD 的厚度與驅動電壓進行調控。OLED 與 LED 元件壽命之研究顯示自製的 UV 硬化 Silicone-acrylate 封裝樹脂具有優異阻氣性，可將 OLED 與 LED 元件的半衰壽命（Half-lifetime）自未封裝之 9 小時與 2400 小時提高至 98 小時與 18300 小時。

本論文研究同時製備高熱穩定性、適度接著強度與優異阻氣性的 UV 硬化環氧樹脂-壓克力奈米複合膠材（Epoxy-acrylate Nanocomposite Resins），膠材中除奈米氧化矽填充物之外，並添加 Invar 合金，以提高其阻氣性並減低了於 UV 硬化後的收縮問題。此一膠材被應用 OSCs 的封裝，實驗結果顯示其可有效阻擋空氣中水氣與氧氣入侵元件中，而提升 OSCs 元件的壽命。

本論文同時研發以 聚乙烯接枝甲基丙烯酸縮水甘油酯 （Polyethane-graft-Glycidylmethacrylate，PE-g-GMA）為相容劑（Compatibilizer）之聚苯硫醚/聚乙烯對苯二甲脂 （Polyphenylene Sulfide/Poly(ethylene terephthalate)/PE-g-GMA，PPS/PET/PE-g-GMA (wt./wt./wt.)=100/50/12.5） 與聚苯硫醚/尼龍 6,6/玻纖合金 （PPS/Nylon 6,6/Glass Fiber Alloy/ PE-g-GMA(wt./wt./wt./wt.) =100/50/45/12.5）的成型製程以製作 LED 之耐溫構裝反射杯體，PE-g-GMA 含量對高分子合金之影響以及製成價廉、高反射性質之耐溫構裝反射杯體之可行性亦被分析之。

A Study on the Properties and Modification of Encapsulating Materials for Photoelectric Devices

Student: Chen-Ming Chen   Advisor: Dr. Tsung-Eong Hsieh

Department of Materials Science and Engineering, National Chiao Tung University

Abstract

This thesis studied the preparation of various ultraviolet (UV)-curable polymeric composite resins (i.e. PU-acrylate/silica (weight ratio = 90 wt.%/10 wt.%), silicone-acrylate/Alumina (weight ratio = 90 wt.%/10 wt.%) as well as epoxy-acrylate/silica/Invar (weight ratio = 35 wt.%/50 wt.%/15 wt.%) and their applications for the packaging of organic light-emitting devices (OLEDs), organic solar cells (OSCs) and light-emitting diodes (LEDs). In the part of study relating to OLEDs, the lifetimes of devices were successfully enhanced by modulating the LiF thickness and utilizing the UV-curable silicone-acrylate adhesives for encapsulation. It was found that the LiF and lab-made encapsulating adhesives can effectively block the invasion of moisture as well as oxygen in the atmosphere into the OLEDs so that an 18-folds increment of lifetimes was achieved after encapsulation. A low turn-on voltage (3 V), high luminance (4850 cd/m^2 at 9 V), color/luminance tunable OLED with device structure as ITO glass/naphthyl phenyl benzidine (NPB; 80 nm)/4,4'-bis(diphenylvinylenyl)- biphenyl (ADS082BE; 35 nm)/1,3-bis[2-(2,2'-bipyridine-6-yl)-1,3,4-oxadiazo-5-yl] benzene (Bpy-OXD; 20 nm)/tris-[8-hydroxy- quinoline]aluminum (Alq$_3$; 50 nm)/lithium fluoride (LiF; 3 nm)/aluminum (Al; 80 nm) was successfully fabricated in this study. Its

electroluminescent properties (*e.g.*, hue, luminescent intensity, *etc*.) could be modulated by the manipulation for the layer thickness of NPB/ADS082BE/Bpy-OXD and the applied bias. In addition, the UV-curable silicone-acrylate encapsulating resin exhibited excellent gas barrier capability so that the half-lifetimes of OLEDs and LEDs reached 98 and 18300 hrs while those without encapsulation were only 9 and 2400 hrs.

The UV-curable epoxy-acrylate nanocomposite resins with good thermal stability, moderate adhesion strength and excellent gas barrier capability were also prepared in this work. In order to improve the gas blocking properties, the Invar alloy was also blended into the resins so as to increase the gas resistance and decrease resin shrinkage after UV curing. Experimental results revealed that introduction of epoxy-acrylate nanocomposite resins could effectively block the penetration of moisture as well as oxygen in the air into the devices and consequently promoted the lifetimes of OSCs.

Fabrication of polymeric reflector cups for LEDs by using polyphenylene sulfide/poly(ethylene terephthalate) (PPS/PET) and PPS/nylon 6,6/glass fiber alloys *via* injection molding process was also presented in this work. In order to enhance their mechanical properties, the compatibilizer, PE-g-GMA, was first developed by grafting the glycidyl methacrylate (GMA) into the low-density polyethylene (LDPE) with initiators by reactive extrusion procedure in a twin screw extruder. PPS/PET and PPS/nylon 6,6/glass fiber alloys with various amounts of PE-g-GMA (PPS/PET/PE-g-GMA (wt./wt./wt.)=100/50/12.5; PPS/Nylon 6,6/Glass Fiber Alloy/ PE-g-GMA(wt./wt./wt./wt.) =100/50/45/12.5) were then prepared and their physical properties as well as feasibilities for the high-brightness LEDs were also analyzed.

誌　謝

感謝師長及實驗室夥伴的長期支持與鼓勵，願以此文獻給我敬愛的父親。

Contents

Figure Captions

x

Table Captions

Chapter 1

Introduction

Organic Light-emitting devices (OLEDs) are one of the important types of flat panel displays (FPDs) due to the advantages of low cost, low power consumption, high contrast ratio, fast response time, high brightness and large viewing angles [2-6]. However, invasion of moisture/oxygen may cause the oxidation of the active metal electrode as well as the thermal degradation of organic light-emitting layer during device operation. It drastically deteriorates the lifetime of OLEDs and hence a unique hermetic sealing method is required [7,8].

The demand of hermetic sealing similarly occurs in the packaging of organic solar cells (OSCs). At present, most of the researches focus on the improvement of the efficiency for solar cells; the studies relating to the packaging techniques and improvement of device lifetime are relatively less. One of the purposes of this thesis work is to develop the ultraviolet-curable (UV-curable) sealing adhesives for the packaging of above photoelectronic devices in terms of the concept of nanocomposites. In this study, we successfully synthesize several UV-curable nanocomposites and applied them for the packaging of OLEDs and OSCs. The experimental results reveal that lab-made nanocomposites exhibit good gas barrier capability, therefore prolonging the lifetimes of OLEDs and OSCs.

Light emitting diodes (LEDs) possess a widespread utilization in the fields of displays and solid-state lighting. Though inorganic, encapsulation is inevitable to ensure good reliability of LEDs for various applications. UV-curable transparent organic/inorganic hybrid nanocomposites with good adhesive strength, fast curing speed, moderate hardness, high refractive indices, and excellent gas resistance was successfully prepared and utilized for the encapsulation of LEDs, substantially

extending their lifetimes.

Furthermore, the aluminum (Al) reflector cups of LEDs exhibit the disadvantage of high cost and insufficient reflection ratio. This work also presents polymeric-type reflector cups with low cost, high reflection ratio and easy processing method. In this part of study, polyphenylene sulfide/poly(ethylene terephthalate) (PPS/PET) and PPS/nylon 6,6/glass fiber alloys are adopted as the base materials for the fabrication of reflector cup samples. In order to enhance their mechanical properties, the compatibilizer, PE-g-GMA, was first developed by grafting the glycidyl methacrylate (GMA) into the low-density polyethylene (LDPE) with initiators by reactive extrusion procedure in a twin screw extruder. PPS/PET and PPS/nylon 6,6/glass fiber alloys contained various amounts of PE-g-GMA was then prepared and their physical properties and feasibility to the high-brightness LEDs are analyzed.
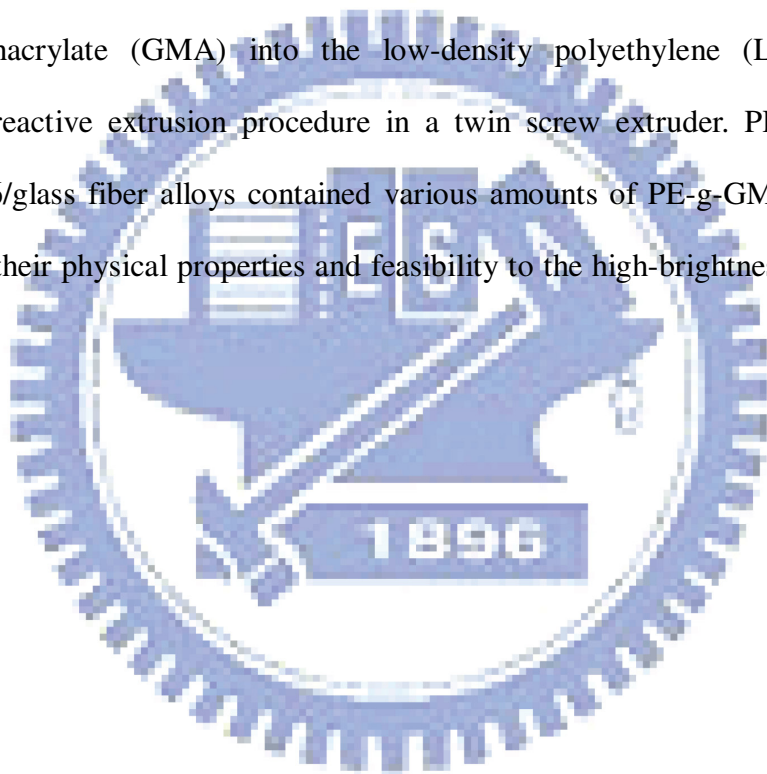
Chapter 2
Literature Review

2.1. Overview of Electronic Packaging Technology

Integrated circuits (ICs) and optoelectronic devices are made in rather dedicate manner that a supporting/protective structure is demanded in order to prevent possible damages from environment and shipping/handling during subsequent assembly process. The way to achieve such purposes, known as electronic packaging technology, is in essential to all kind of electronic products to ensure a certain level of reliability during their usage and/or operation. According to materials used and the encapsulating structure, electronic packaging can be categorized as metal packaging, ceramic packaging, and plastic packaging [9]. Among these, metal packaging and ceramic packaging are termed as hermetic packaging while plastic packaging is ascribed to the non-hermetic packaging since the highly dense microstructures of metals and ceramics enable good gas/moisture block effects in comparison with polymeric materials. However, ceramic packaging is an expensive technology since its substrate preparation and metallization processes are extremely complicated. The sealing methods for metal packaging and ceramic packaging are similar, *e.g.*, welding, brazing, soldering or glass frit sealing; however, in spite of welding, all of them require a relatively high processing temperatures. For instance, the temperatures of soldering and glass frit sealing are as high as 200 and 400°C, respectively, which are inapplicable to the encapsulation of advanced optoelectronic products such as organic light-emitting devices (OLEDs) and organic solar cells (OSCs). Furthermore, soldering and brazing might leave flux in the encapsulation, reducing the reliability of products. A fatal point of metal packaging and ceramic packaging is the difficulty to reach the light and thin packaging profiles, which is opposite to the developing trend

of contemporary electronic products.

It seems plastic packaging with the advantages such as low cost and miniaturization is the only choice for the packaging of OLEDs and OSCs, nevertheless, conventional plastic packaging utilizing thermal molding process remains inappropriate since OLEDs and OSCs cannot tolerate the severe processing conditions, *e.g*., high temperature, long curing duration and high pressure, during the molding process. An alternative way is to use the ultraviolet (UV)-curable resins with fast curing rate and low processing temperatures to avoid the device deterioration resulted from the thermal degradation. The encapsulation using UV curing technology hence becomes the viable way for the packaging of OLEDs and OSCs.

Acrylics resins [10] are well-known polymeric materials since they exhibit fast curing rate, high structural strength and excellent processing convenience. Their fast curing performances are suitable for specific electronic applications such as the bonding of magnets into speaker assemblies and others with high assembly line speed. Furthermore, they can be cured with heat or UV irradiation [11,12] by the addition of thermal initiators or photoinitiators, respectively. UV-curable acrylics resins have shorter curing time, weaker structure strength, and higher contraction than thermal curable ones. Although acrylics resins are good candidates for polymer matrices of organic/inorganic hybrid nanocomposites, they exhibit low viscosity. This severely restricts their practicability.

Epoxy resins [10] are also well-known polymeric materials for encapsulation because of their chemical modifiability, high transparency, good thermal stability and moderate viscosity. They are widely used in electronic, mechanic and biological industrials since the oxirane groups of epoxy resins are active to various functional groups such as alcohol, thiol, anhydride, amine, *etc*., facilitating the curing reactions. They can be cured with heat or UV irradiation [13] by the addition of thermal curing

4

agents or photoinitiators, respectively. Compared with UV curable epoxy resins, thermal curable ones have longer curing duration and the color stains when they are cured at high temperature. Despite the epoxy resins have many merits as the polymer matrices of organic/inorganic hybrid nanocomposites; they exhibit low curing rate and high brittleness after curing.

As described above, acrylics resins possess low viscosity and high contraction after curing. However, epoxy resins exhibit moderate viscosity and low contraction after curing. In addition, epoxy resins have long curing time and high brittleness after curing. Oppositely, acrylics resins possess high curing speed and low brittleness after curing. Thus, we chose these two complementary materials as the polymer matrices to modulate the physical, chemical and mechanical properties and evaluated they applicability to the encapsulation of OLEDs and organic solar cells.

2.2. Introduction to OLEDs and Their Packaging Methods

As shown in Fig. 2-1, typical OLEDs comprise of the glass substrate with indium tin oxide (ITO; anode electrode), hole-transport layer, light-emitting layer, electron transport layer, and cathode electrode [14]. The anode electrode, which may be ITO or
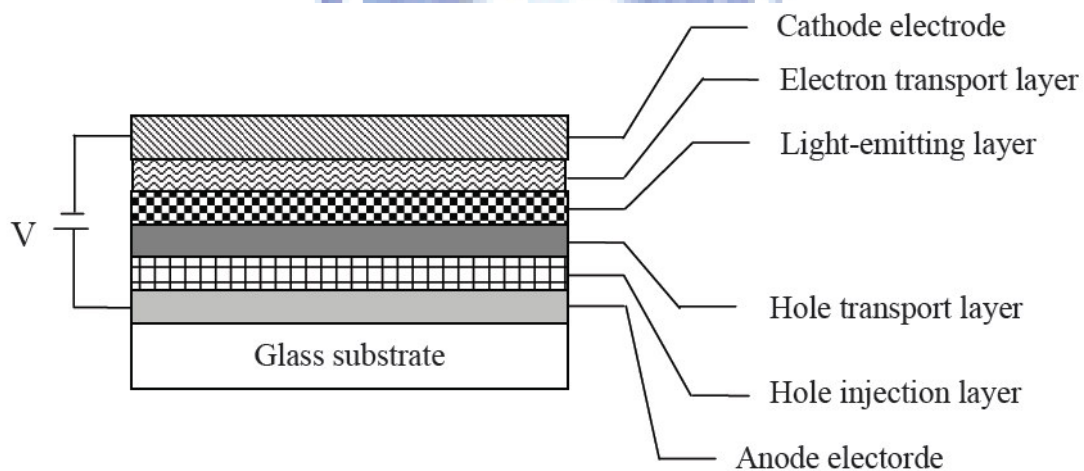
Fig. 2-1. Typical OLED structures.

ITO/poly(ethylenedioxy)thiophene (PEDOT) is conducting material with good

transparency and high hole injection capability. Moreover, the hole transport layer like naphthyl phenyl benzidine (NPB) is to diminish the energy gap between anode electrode and hole transport layer and to increase the thermal resistance [15].

OLEDs have attracted a lot of research interests because of their promising applications in flat panel displays (FPDs), solid-state lightings, *etc*. Compared with other competitors, *e.g.*, liquid crystal displays (LCDs), OLEDs possess the advantages of low cost and power consumption, high contrast ratio and brightness, fast response time and large viewing angles [2-6]. For full color applications, many organic light-emitting materials have been reported. Tris-[8-hydroxyquinoline] aluminum (Alq$_3$) and triaryl amine have been used as emitting layer and hole transport layer respectively by Tang and Van Slyke [14]. With these two materials, the first thin-film OLED was successfully fabricated. Alq$_3$ has been found to be a singlet host material in the guest-host doped emitter systems and capable of blending with other dopants to give off full colors (*e.g.*, Alq$_3$/coumarin mixture can be modulated to irradiate blue, orange, and green emissions.). In addition, anthracene and its derivatives have been reported to be blue emitting layers for OLEDs [16]. The requirements for cathode electrode are low work function and excellent electron injection properties (*e.g.*, Ca, Ag, Al, Al/Li, Mg, Mg/Ag, *etc.*). Nonetheless, these metals cannot be exposed in the air ambient during device actuation owing to their high chemical activity. Furthermore, organic layers for OLEDs, *e.g.*, hole-transport layer, emitting layer, electron transport layer, *etc.*, erode during device operation while the oxygen and moisture in the atmosphere penetrate into the devices [17]. Deterioration of metal electrode and organic materials causes dark spots when the device is lighted up and drastically decreases its lifetime [7,18]. Consequently, a hermetic encapsulation is necessary for OLEDs.

Figure 2-2 depicts the cross-sectional view of the encapsulating structure of

6

OLEDs. The sealing is in fact achieved by dispersing the UV-curable resin around the active region of the device, a glass or metal lid is then flipped on the substrate, followed by a proper UV-curing treatment to accomplish the sealing. The packaging procedure is usually carried out in the atmosphere with dry nitrogen/argon or in the dry ambient (<1 ppm v/v; dew point = −76°C) [19]. In order to absorb the residual oxygen/moisture in the encapsulation or the undesired substances permeating through the encapsulating adhesive, the desiccant (*e.g*., calcium oxide or barium oxide) is also applied on the device side of lid [14]. Moreover, a post-thermal curing at 80°C for 1 hr is necessary to suppress the photo-polymerization, raise the crossing density, and reduce residual stress of encapsulating adhesives. Since polymeric materials exhibit less resistance to oxygen and moisture, modification of resin structure is thus indispensable to enhance the gas barrier property so as to ensure a reliable performance of OLEDs.
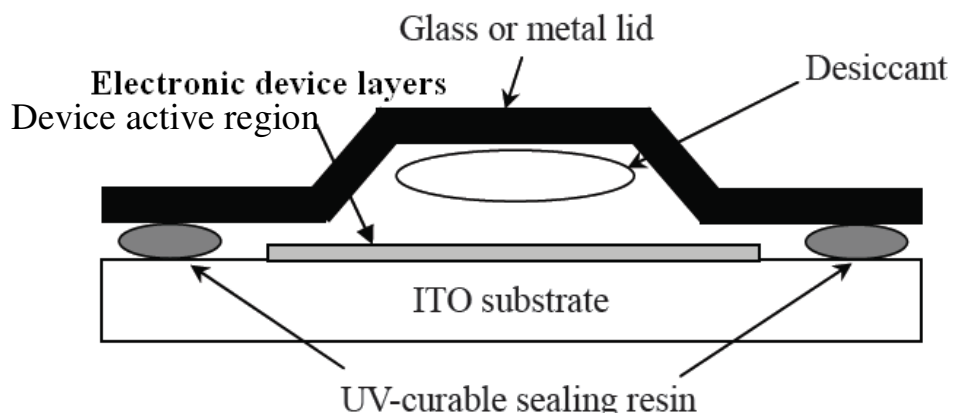
Fig. 2-2. Encapsulating structure for OLEDs.

In recent years, the developments of OLEDs have been switched to top-emitting OLEDs (TOLEDs) and flexible OLEDs (FOLEDs). However, FOLEDs cannot be packaged with metal or glass lid owing to their rigidity and TOLEDs with the metal lid are not transparency. Therefore, utilization of polymeric encapsulating adhesives is

a potential solution. Fig. 2-3 [17] manifests the packaging procedure with transparent organic/inorganic barrier coating for FOLEDs.
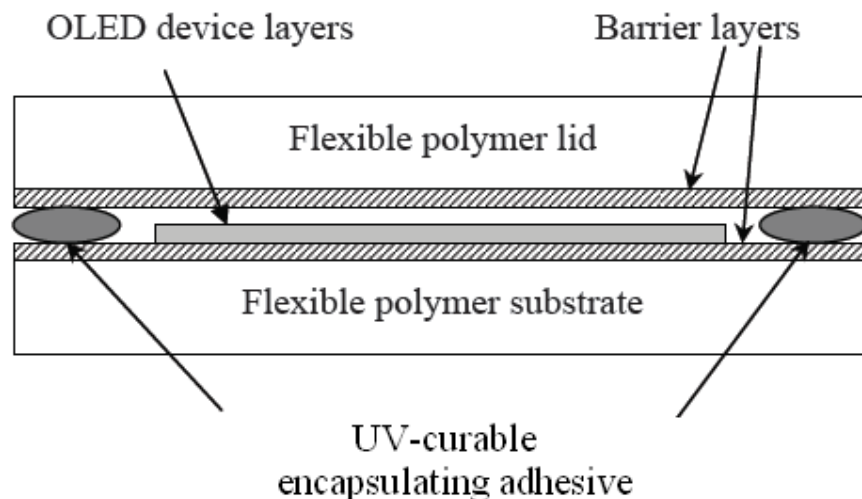
Fig. 2-3. Encapsulating structure of FOLEDs for OLEDs with transparent organic/inorganic barrier coatings.

2.3. Introduction to OSCs and Their Packaging Methods

Although silicon-based solar cells have been found to exhibit good efficiency for the conversion of sunlight into electrical energy, their cost is relatively high. In recent years, OSCs have become alternative candidates for photoelectric conversion because of low cost and good processability. Nevertheless, the lifetime of OSCs has been a hindrance for the commercialization since oxygen and moisture in the air erode the organic materials and metal electrodes of devices, dramatically dropping the lifetime [8]. In addition, most researches focus on the improvements of OSC efficiency but the studies relating to device lifetime promotion are relatively less.

Poly(3-hexylthiophene) (P3HT) possesses good filming and excellent semiconductor characteristics such as higher carrier mobility, so that it can be applied onto a flexible plastic substrate to fabricate electro-optical devices. It can also be applied to multilayer structures according to the device requirements [20]. In 1995,

Heeger *et al.* used MEH-PPV mixed with [6,6]-phenyl C_{61}-butyric acid methyl ester (PCBM) to form a bulk heterojunction structure and obtained power conversion efficiency (PCE) of 1.5 % [21]. In 2001, Sariciftci *et al.* used MDMO-PPV mixed with PCBM employing LiF/Al as the cathode in an OSC and increased its PCE to 2.1 % [22]. In 2005, Yang *et al.* used the self organization effect in the active layer and a "slow growth" treatment to reduce the resistance of components in series connection. The carrier mobility of holes was increased and PCE raised to 4.37% [23]. In 2005, the PCE of OSC reached 5% mainly resulted from the usage of materials such as P3HT/PCBM to prepare the *p-n* junction structure [24]. Such kinds of OSCs exhibit the advantages of low-cost, lightweight, flexibility, and large-area processability [25]. In 2007, Jin *et al.* integrated the best processing conditions and added glycerol within the buffer layer to increase the short-circuit current density and PCE to 4.64% [26].

Although the literatures relating to the lifetime promotion of OSCs using metal or glass lid for encapsulation have been reported [27-29], the packaging process is rather complicated and expensive. Recently, inorganic materials such as SiO_2 and Al_2O_3 [30], polymers such as polyacrylics, PET, and poly(p-xylylene) [31,32] and their combinations such as organic/inorganic hybrid composites [33] have been reported for the gas barrier application. Nevertheless, the lifetimes of OSCs packaged with these materials remain unsatisfied.

2.4. Introduction to LEDs and Their Packaging Methods

Light emitting diodes (LEDs) and relating products are widely utilized in displays and illuminations. Similarly, LEDs require packaging structures to prevent the erosion of metal electrode and chip induced by the invasion of moisture and oxygen in the air so as to secure a satisfactory lifetime [7]. Epoxy resins is the most common materials for LED package [10] and the encapsulating structure of LEDs is

9

manifested in Fig. 2-4.
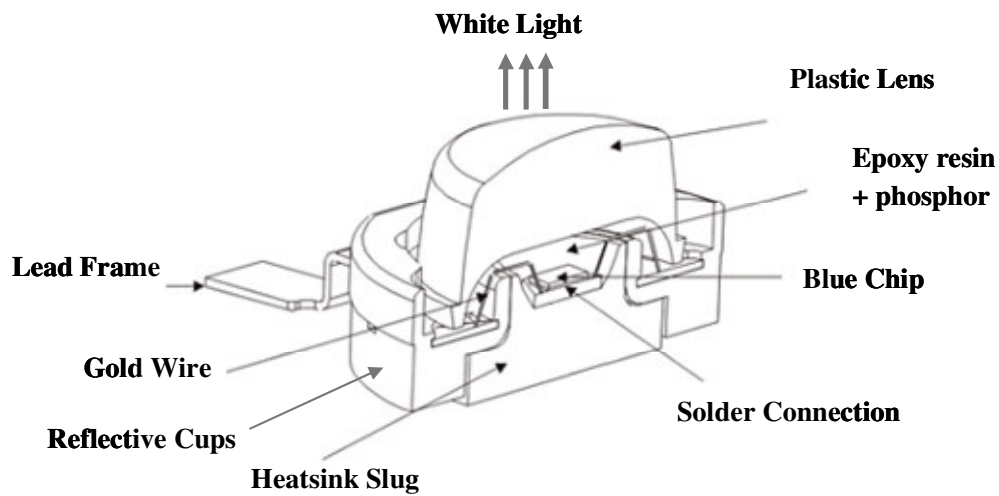
Fig. 2-4. Encapsulating structures for LEDs.

In order to modulate the shape of light, the reflector cups for LEDs are needed. Aluminum (Al) possesses high reflecting property so that the Al cups are extensively used for the modulation of LEDs. Nevertheless, the cost of LEDs with Al cups is high and it results undesired harsh lights.

Polyphenylene sulfide/poly(ethylene terephthalate) (PPS/PET) and the PPS/nylon 6,6 have become engineering plastics with widespread applications such as electronic parts, construction parts, *etc*. because of their good mechanical properties, high thermal stability, facile processibility and low cost. Recently, they are found to possess excellent reflectivity and are promising materials for reflector cups of LEDs. Nevertheless, phase separation often takes place in the cases of PPS/PET and

PPS/nylon 6,6, causing inhomogeneous blend and deteriorating the physical properties. A compatibilizer is hence required in order to solve this problem. One of the purposes of this work is to study the effects of compatibilizer types on the blending process and physical properties of PPS-based materials so that they applications to LED packaging can be realized.

2.5. Applications of Nanocomposites to Packaging of Electronic Devices

Organic/inorganic hybrid nanocomposites, which are composed of polymer matrices and inorganic fillers, have attracted lots of attentions for several decades because of their versatility in physical/chemical properties. They are used for the preservation of food as well as beverages because of the good resistance to the penetration of oxygen as well as moisture in the atmosphere [1]. Pure polymers, such as acrylics and epoxy resins, have been extensively applied for the polymer matrices of organic/inorganic hybrid nanocomposites due to their low cost, high processing facility and moderate toughness. In order to enhance the gas barrier performances of polymer matrices, inorganic fillers such as silica, metal oxide, and clay have been added [34-38]. A schematic illustration for the enhancement of oxygen/moisture resistance is shown in Fig. 2-5.
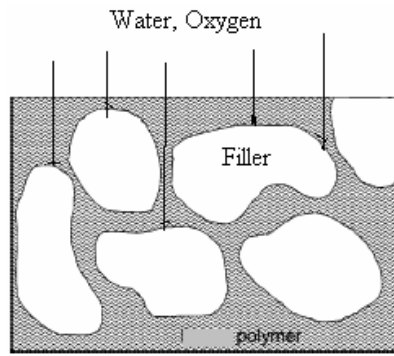
Fig. 2-5. Schematic illustration for the enhancement of oxygen/moisture resistance in

organic/inorganic hybrid nanocomposites.

The inorganic fillers in the nanocomposites may effectively form the gas barrier. Yano *et al.* proposed a gas invasion model in exfoliated polymer/clays nanocomposites [39]. As manifested in Fig. 2-6, the total path of a diffusing gas molecule (d') can be expressed as

$$d' = d + d \cdot L \cdot \frac{V_f}{2W} \qquad (2\text{-}1)$$

where d is the thickness of a nanocomposite film, W is the width of clays, L is the length of a clay, and V_f is the volume fraction of clays. The ratio of the total path to the thickness of a nanocomposite film, the tortuousity factor (τ), is defined as

$$\tau = \frac{d'}{d} \qquad (2\text{-}2)$$

The permeability coefficient of composite (P_C) was therefore obtained as

$$P_C = \frac{P_P}{\tau} \qquad (2\text{-}3)$$

where P_P is the permeability coefficient of the polymer matrix. Because the total path is larger than the thickness of a resin film, the tortuousity factor would be larger than 1 and P_C would hence be smaller than P_P. According to this theory, the extended gas

diffusion path resulted from exfoliated clays in the nanocomposites, reducing the rate of gas permeation and allowing the inorganic filler as a permeation barrier in nanocomposite resins [40].
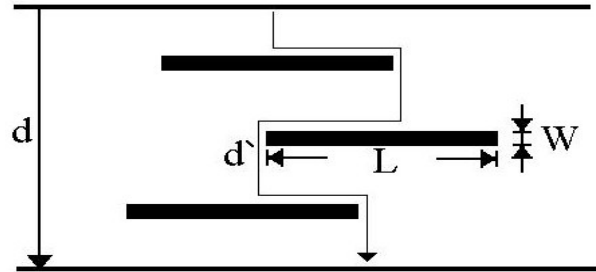
Figure 2-6. A gas diffusion model proposed by Yano *et al.* [39].

2.6. Motivations

Although conventional thermal method has been utilized for the synthesis of encapsulating adhesives, the reaction takes several hours for completion, which is time and energy-consuming. Therefore, fast and effective preparation for package materials has become a crucial topic. Furthermore, the common encapsulating materials exhibit poor gas barrier capability, resulting in insufficient lifetimes while they are applied for package of photoelectric devices. Short lifetimes are pivotal obstacles to their commercialization.

Chapter 3

Experimental Methods

3.1. Encapsulation of OLEDs

3.1.1. Experimental Flow for Encapsulation of OLEDs

The experimental flow for encapsulation of OLEDs was illustrated in Fig. 3-1.

Preparation of OLED
encapsulating adhesives

↓

Preparation of OLED or
Color/Luminance Tunable
OLED samples

↓

Encapsulation by UV
illumination

↓

Characterizations and
Reliability Test
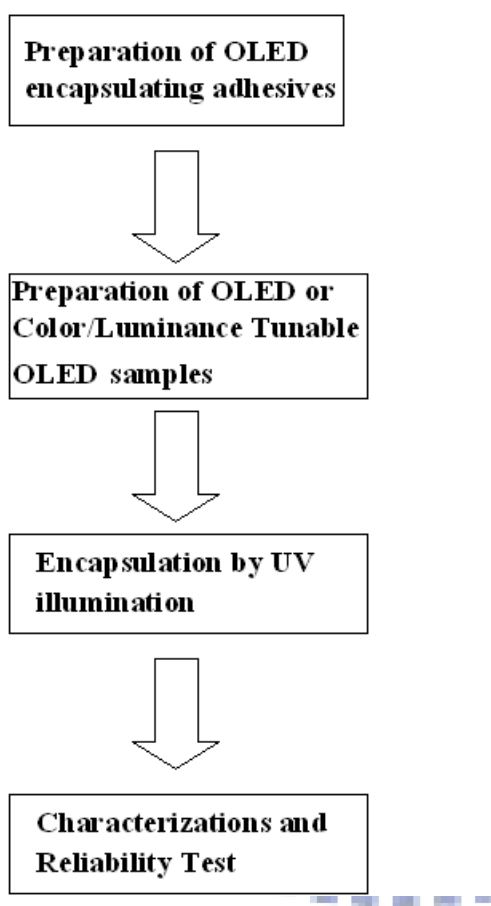
Fig. 3-1. Experimental flow for encapsulation of OLEDs.

3.1.2. Materials for OLED Encapsulating Resins

Figure 3-2 illustrates the chemical structures of monomers for the preparation of UV-curable OLED encapsulating resins including PU-acrylate and silicone-acrylate. All chemicals were obtained from UCB Co. and used without further purification. Silica and alumina inorganic fillers with sizes = 30 to 100 nm were obtained from

14

Aldrich Co.
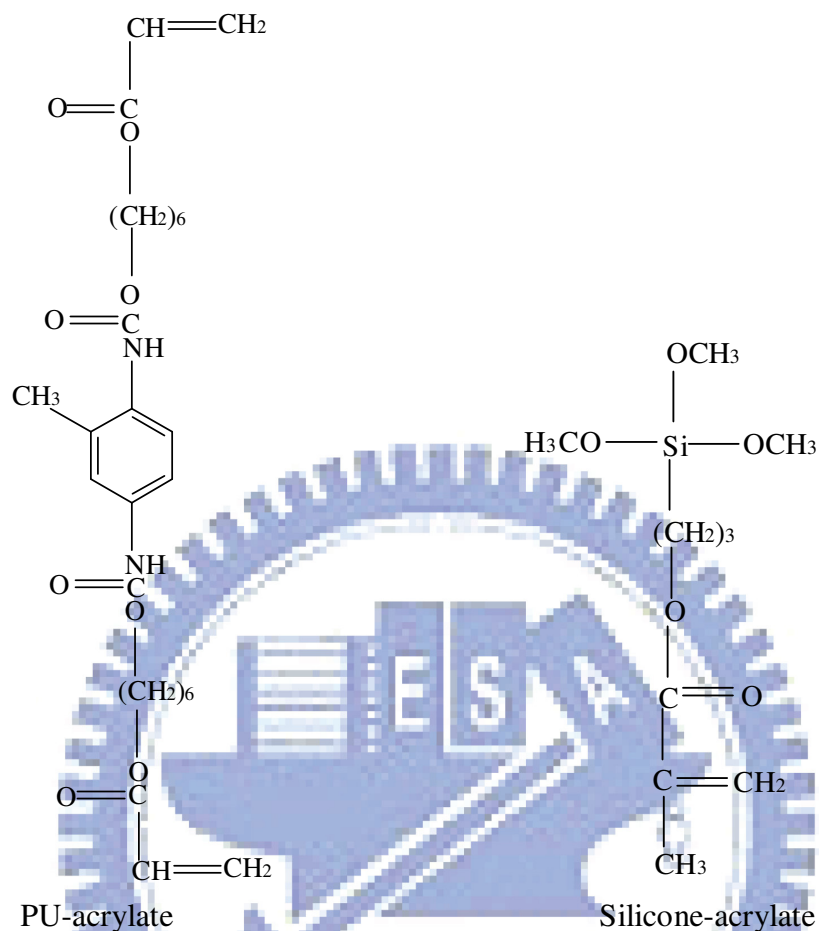
Fig. 3-2. Chemical structures of monomers for the preparation of UV-curable OLED encapsulating resins.

The initiators (benzoyl peroxide; BPO) and photoinitiators (Irgacure 184/Irgacure 369/Irgacure ITX/Irgacure 651/Darocur 1173/Irgacure 819/triaryl sulfonium hexafluoroantimonate) for the preparation of UV-curable OLED encapsulating resins were purchased from Aldrich Co. and Ciba Co., respectively. Their chemical structures are depicted in Fig. 3-3 and were utilized without further purification. The initiators and photoinitiators were also adopted for the preparation of encapsulation resins for solar cell and LED samples.
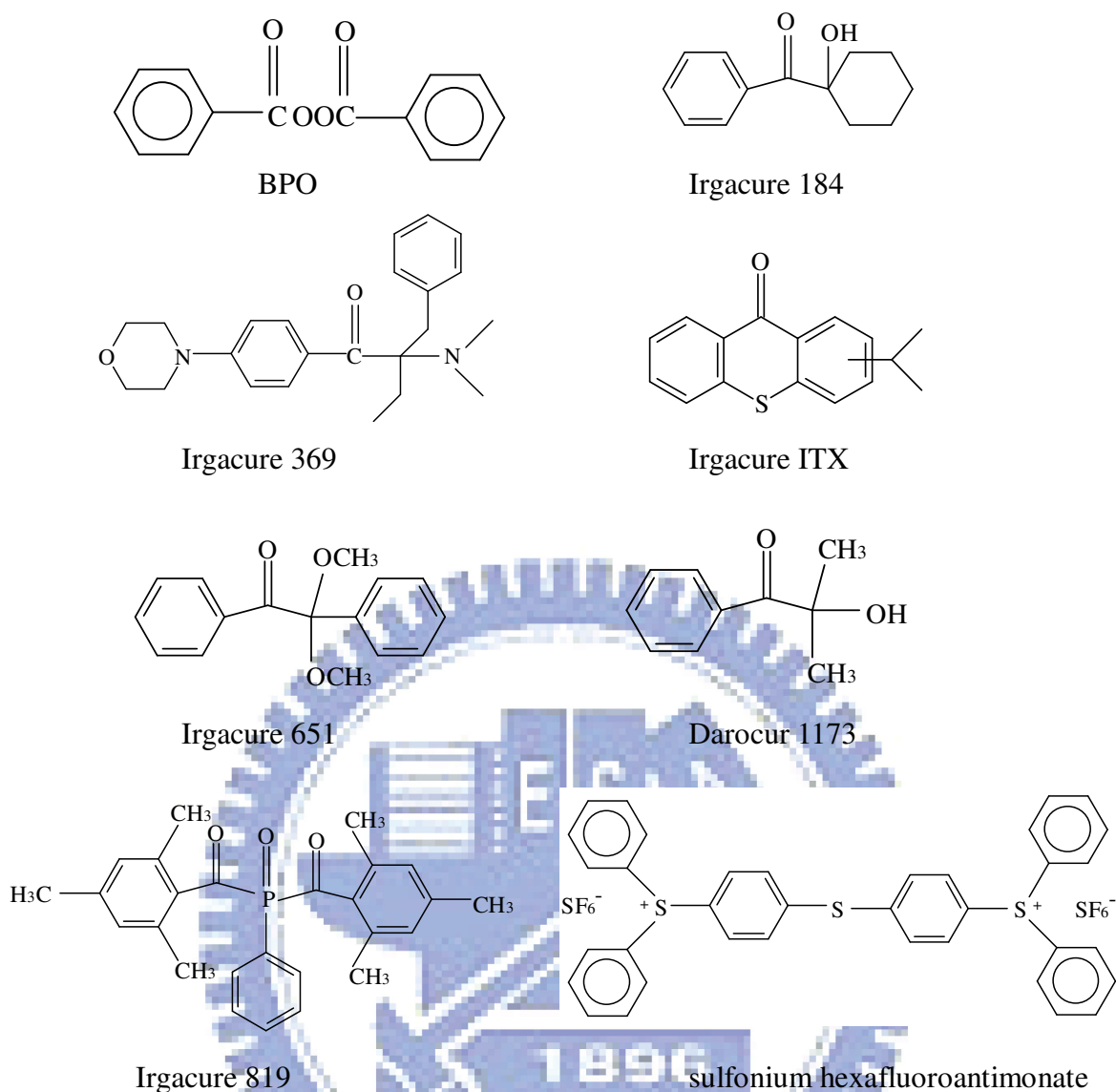
Fig. 3-3. Initiators and photoinitiators for the preparation of UV-curable OLED encapsulating resins.

3.1.3. Preparation of OLED Encapsulation Resins

3.1.3.1. Synthesis of UV-curable PU-acrylate

PU-acrylate monomer (90 g), silica (10 g), Irgacure 184 (1 g), Irgacure 369 (0.5 g), and Irgacure ITX (0.5 g) were stirred for 30 min and irradiated by a UV lamp (100 W) for 10 min (Scheme 1). The weight-average molecular weight (M_w),

16

number-average molecular weight (M_n), M_w/M_n ratio and viscosity of PU-Acrylate were 153,000, 72,600, 2.11, and 16,300 cps, respectively.

Scheme 3-1
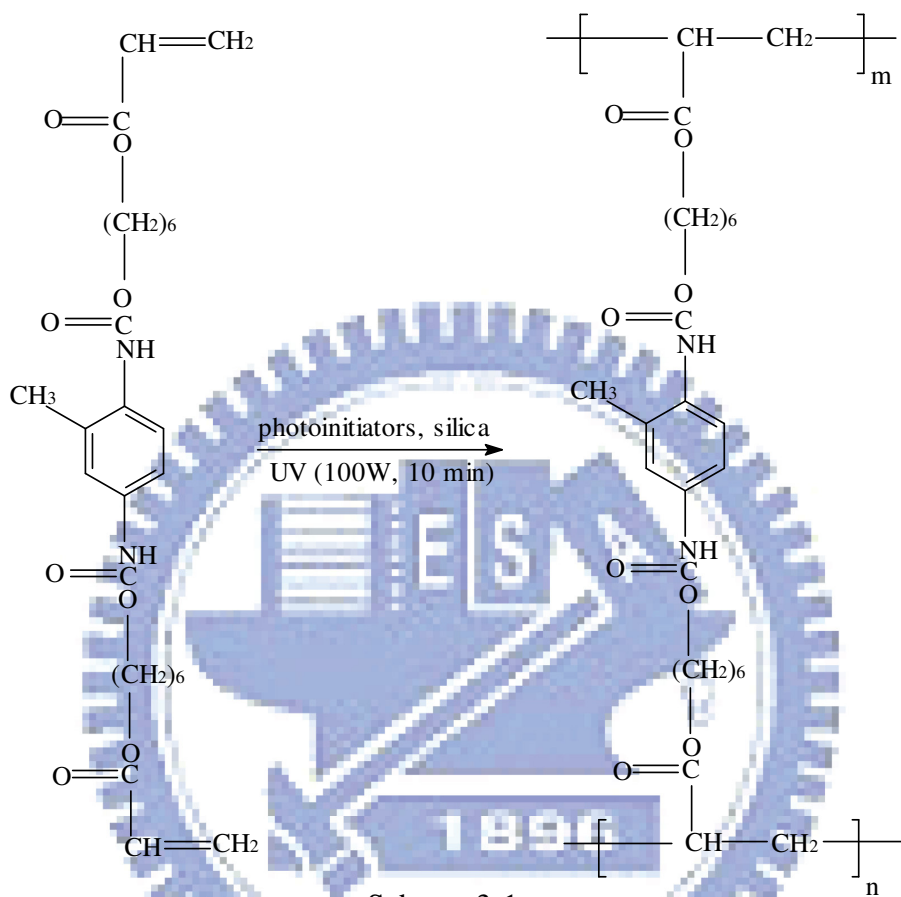
3.1.3.2. Synthesis of UV-curable Silicone-acrylate

Silicone-acrylate monomer (180 g), Irgacure 651 (2 g), Darocur 1173 (1 g), Irgacure 819 (0.5 g), and alumina (20 g) were mixed for 30 min and illuminated by a UV lamp (Entela UVP; wavelength = 365 nm) at the power of 100 W for 20 min (Scheme 2). The M_n, M_w, M_w/M_n ratio, and viscosity of silicone-acrylate resin were 37,300, 83,200, 2.23, and 7,200 cps, respectively.

OCH₃ ... OCH₃ reaction scheme with I-651, D-1173, I-819, alumina; UV(100W, 20 min)
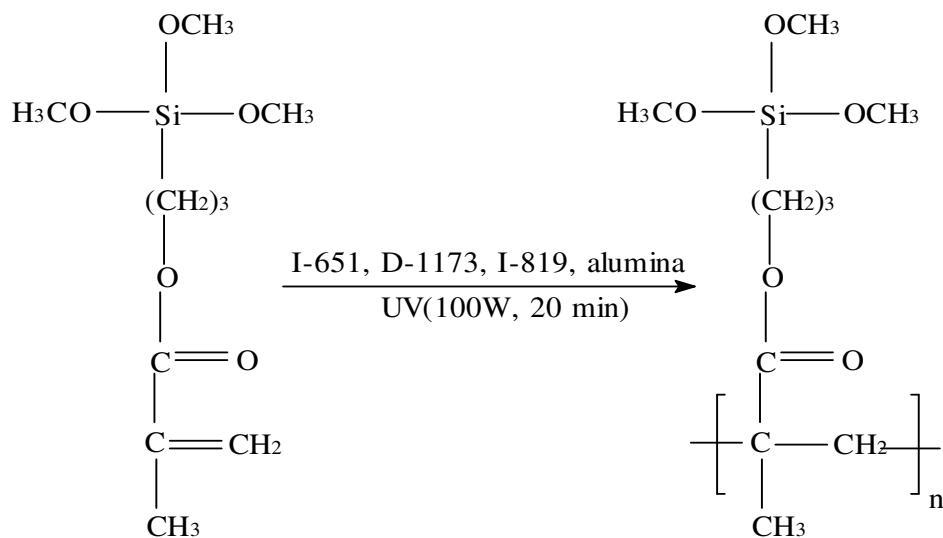
Scheme 3-2

3.1.4. Materials for OLED Samples

The materials for OLED sample preparation include naphthyl phenyl benzidine (NPB; hole transport material), tris-[8-hydroxyquinoline] aluminum (Alq₃; light emitting material), LiF (electron injection/protection material), 4,4'-bis(diphenyl vinylenyl)-biphenyl(ADS082BE; blue-color emitting material), 1,3-bis [2-(2,2'-bipyridine-6-yl)-1,3,4-oxadiazo-5-yl]benzene (Bpy-OXD; electron blocking material). Their chemical structures are showed in Fig. 3-4. All chemicals were purchased from Aldrich Co. and used without further purification.

NPB
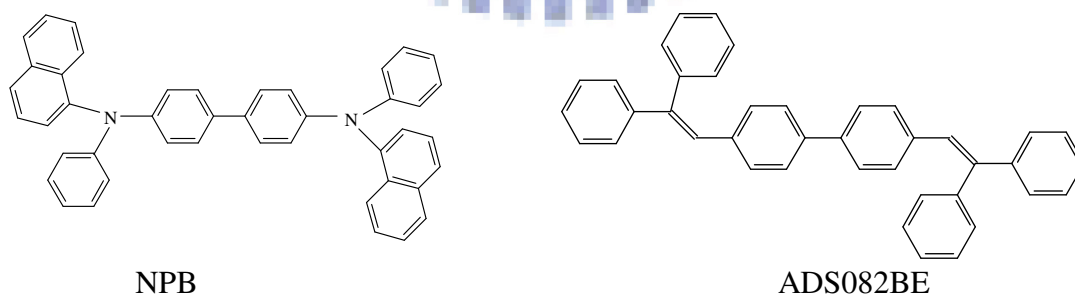
ADS082BE

Fig. 3-4. Chemical structures of NPB, ADS082BE, Bpy-OXD, and Alq₃. (continued on next page.)
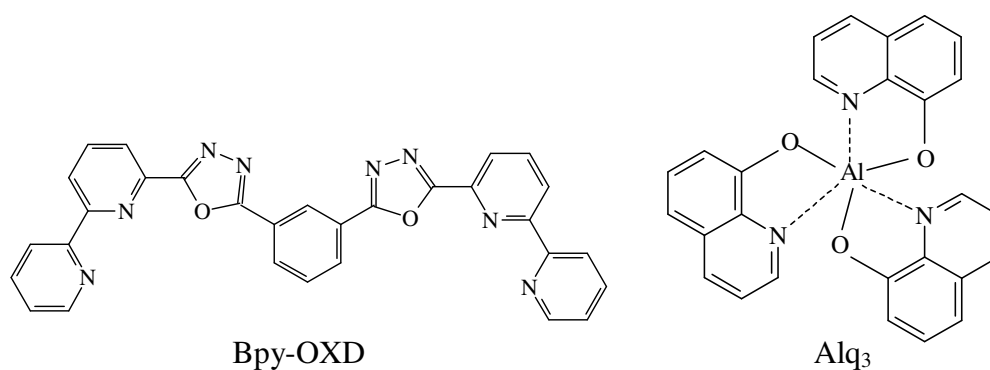
Bpy-OXD   Alq₃

Fig. 3-4. Chemical structures of NPB, ADS082BE, Bpy-OXD, and Alq₃.

3.1.5. Preparation of OLED Samples

The OLED samples were fabricated in a glove box. Firstly, the ITO glass substrate (sheet resistance = 5 Ω/) was ultrasonically cleaned with the acetone, methanol, and de-ionized water for 5 min. After dried with a stream of nitrogen, baked in a oven at 120°C for 30 min and treated by O_2 plasma for 90 sec, NPB (hole transport layer; 50 nm), Alq₃ (light emitting layer; 50 nm), LiF (electron injection layer; 3 nm) and Al (cathode; 80 nm) were sequentially deposited onto the ITO glass by using a vacuum evaporator (ULVAC VPC-060) schematically illustrated in Fig. 3-5. The deposition conditions are: background pressure = 4×10^{-6} torr; deposition rate of organic materials = 0.3-0.5 Å/sec; deposition rate of LiF and Al = 2-5 Å/sec. The structure of such a sample is illustrated in Fig. 3-6(a) and is denoted as Type 0 sample. In order to investigate the gas barrier effect of the LiF protection layer, 80- and 100-nm thick LiF layers were further deposited on the Type 0 sample. It was termed as Type I sample and its structure is depicted in Fig. 3-6(b). The Type II sample shown in Fig. 3-6(c) is achieved by encapsulating the resin prepared previously *via* spin coating process (stage I: 1,500 rpm for 20 sec; stage II: 3,500 rpm for 30 sec). The thickness of encapsulating resins was about 100 μm and afterward, the curing was achieved by UV irradiation for 10 sec in a UV oven (Entela UVP 2450 W). Moreover, the device sizes are 1 cm × 1 cm.
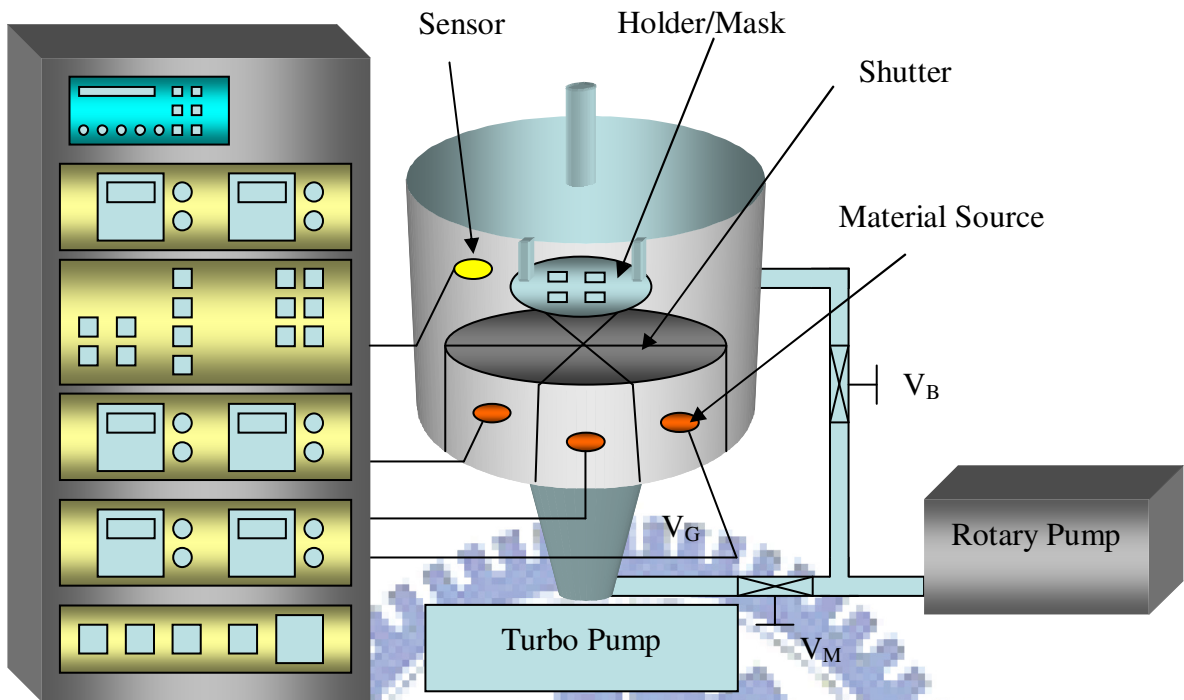
Fig. 3-5. The vacuum evaporation system for OLED sample preparation.

| (a) | (b) | (c) |
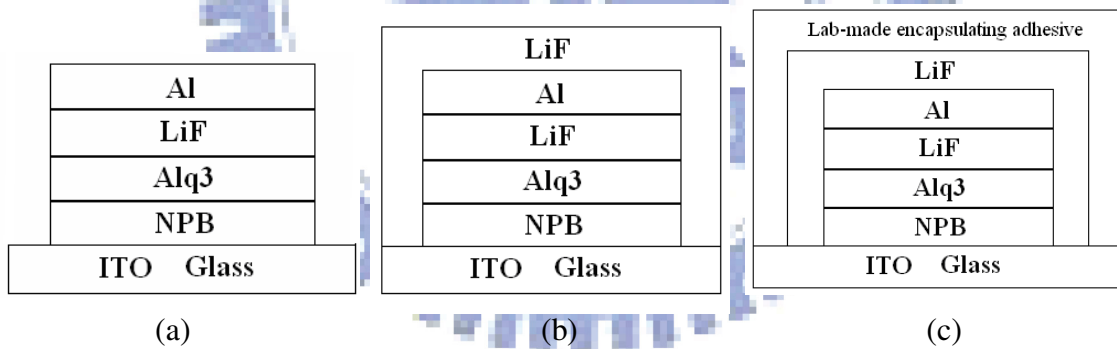
Fig. 3-6. Structures of (a) Type 0; (b) Type I and (c) Type II OLED samples.

3.1.6. Preparation of Color/Luminance Tunable OLED Samples

Firstly, the ITO glass substrate (sheet resistance = 5 Ω/ ; substrate size = 5 cm ×
5 cm) was ultrasonically cleaned with the acetone, methanol as well as de-ionized
water for 5 min and dried with a stream of nitrogen followed by baking in an
120°C-oven for 30 min. After treated by oxygen plasma for 90 sec, NPB (50 or 80

nm), ADS082BE (35 or 50 nm), Alq$_3$ (50 nm), LiF(3 nm), and Al (80 nm) were sequentially deposited on the ITO glass by a vacuum evaporator illustrated in Fig. 3-5. Such a sample was designated as Device III and is illustrated in Fig. 3-7(a). The similar procedure was carried out to prepare the Device IV containing Bpy-OXD electron blocking layers with various thickness (10, 20 or 30 nm) as illustrated in Fig. 3-7(b)).

The silicone-acrylate was subsequently adopted for the encapsualtion of Device IV containing 20-nm thick Bpy-OXD *via* spin-coating technique (stage I: 1,000 rpm for 10 sec; stage II: 2,500 rpm for 20 sec) and cured in an UV oven (Entela UVP 2450 W) for 10 sec at room temperature. The thickness of sealing resin was approximately 50 μm measured by a surface profiler (TENCOR P-10). Such a sample was termed as Device V as shown in Fig. 3-7(c).

Al
LiF
Alq$_3$
ADS082BE
NPB
ITO glass

↓ Light

(a)

Al
LiF
Alq$_3$
Bpy-OXD
ADS082BE
NPB
ITO glass

↓ Light

(b)

Encapsulating adhesive
Al
LiF
Alq$_3$
Bpy-OXD
ADS082BE
NPB
ITO glass

↓ Light

(c)
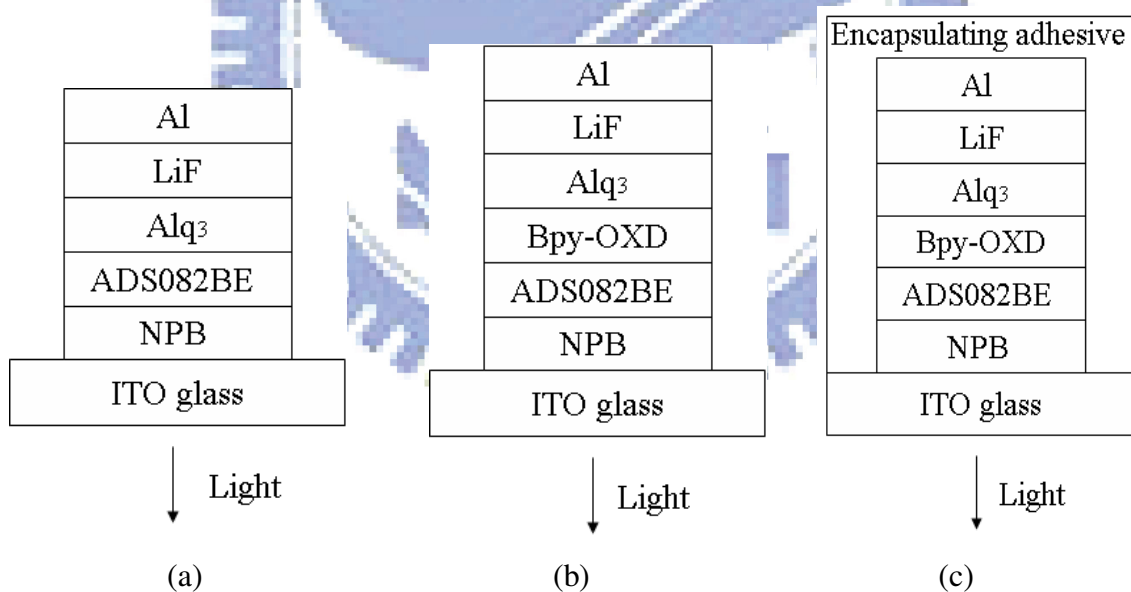
Fig. 3-7. The structures of color/luminance tunable OLEDs. (a) Device III; (b) Device IV and (c) Device V.

3.1.7. Characterizations and Reliability Test of OLEDs

We measured the molecular weight, viscosity, and gas permeation rate with a GPC (Waters Alliance GPC V200), a viscosity meter (Viscolite 700), and a gas permeation meter (Illinois-8501), respectively. Moreover, the EL properties and lifetimes of OLEDs were recorded by a Keithley 2400 and Spectrascan PR650, respectively.

3.2. Encapsulation of OSCs

3.2.1. Experimental Flow for Encapsulation of OSCs

The experimental flow for encapsulation of OSCs was illustrated in Fig.3-8.

Fig. 3-8. Experimental flow for encapsulation of OSCs.

3.2.2. Materials for OSCs Encapsulating Resins

All of resin monomers, initiators, solvents and fillers (silica; 30 to 100 nm) used in the experiment were purchased from Aldrich Co. and used without further purification.

1,6-hexanedol diacrylate and 3,4-epoxycyclohexane carboxylode (see Fig. 3-9 for chemcial structures) were the monomers for acrylics and epoxy resins, respectively. BPO and triaryl sulfonium hexafluoroantimonate were utilized as thermal initiators and photoinitiators, respectively. Propylene glycol monomethyl ether acetate (PGMEA) was the solvent. The metal alloy (Invar) purchased from Goodfellow Co. was 64 *wt.%* Fe: 36 *wt.%* Ni alloy with size about 100 nm.
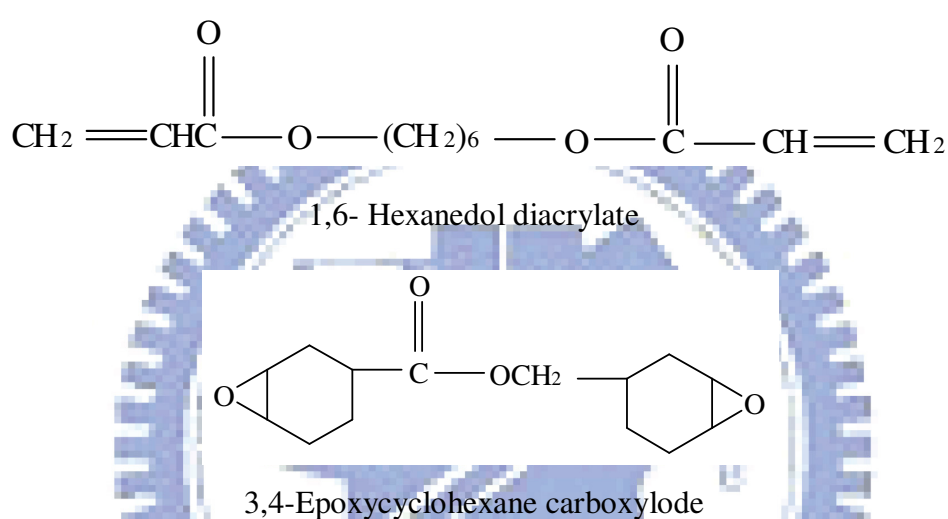
Fig. 3-9. Chemical structures of materials for OSCs encapsulating resins.

3.2.3. Preparation of OSCs Encapsulation Resins

1,6-Hexanedol diacrylate (10 g), benzoyl peroxide (0.1 g), and PGMEA (100 mL) were heated at 100°C for 3 hrs. After blended with 3,4-epoxycyclohexane carboxylode（10 g） and triaryl sulfonium hexafluoroantimonate (0.1 g), the acrylics/epoxy resins (polymer matrices) were obtained. Then, 50 *wt.%* of silica and various amounts of Invar (0-15 *wt.%*) were added into the epoxy-acrylate polymer matrices to form the organic/inorganic nanocomposite resins. The resin sample designation in terms of Invar contents is listed in Table 3-1.

Table 3-1. Designation of resin sample for the encapsulation of OSCs.

Sample designation	Invar content (*wt*.%)
Nanocomposite I	0
Nanocomposite II	5
Nanocomposite III	10
Nanocomposite IV	15

3.2.4. Materials for OSCs Samples

Polyethylene dioxythiophene (PEDOT; hole transport material), Poly(3-hexylthiophene-2,5-diyl)(P3HT; *p*-type semiconductor), and [6,6]-phenyl C61-butyricacid methyl ester (PCBM; *n*-type semiconductor) were acquired from Aldrich Co. and utilized without further purification. Their chemical structures are illustrated in Fig. 3-10.
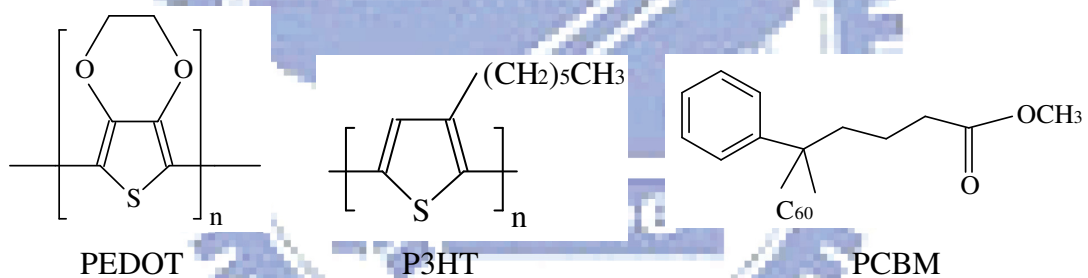
Fig. 3-10. Chemical structures of PEDOT, P3HT and PCBM.

3.2.5. Preparation of OSCs Samples

The ITO glass substrate (sheet resistance = 5 Ω/) was first ultrasonically cleaned with the acetone, methanol, and de-ionized water for 5 min. It was then dried by a stream of nitrogen, baked in a 120°C-oven for 30 min and treated by O_2 plasma for 90 sec. 3 *wt*.% PEDOT was dissolved in water, filtered with a 0.2 µm filter and deposited onto the ITO glass by spin-coating (stage I: 1000 rpm for 20 sec; stage II: 3000 rpm for 30 sec). Afterwards, the P3HT powder (molecular weight = 87,000) was

ground together with PCBM (purity = 98%) to form P3HT/PCBM mixture (weight ratio = 1/1). Then 2 *wt.%* P3HT/PCBM mixture was dissolved in dichloromethane, filtered with a 0.2 μm filter, and deposited onto the PEDOT layer by spin-coating (stage I: 1000 rpm for 20 sec; stage II: 2000 rpm for 30 sec). Finally, the LiF and Al electrode were deposited onto the P3HT/PCBM by vacuum evaporator shown in Fig. 3-5. Figure 3-11(a) illustrates the device structure of solar cell prior to encapsulation.

Encapsulation of organic solar cells was achieved by spin-coating the nanocomposite IV on the top of Al electrode at the condition: stage I: 500 rpm for 10 sec; stage II: 1500 rpm for 20 sec followed by UV curing (Entela UVP 2450 W) for 10 seconds. The thickness of encapsulating layer was about 100 μm. Figure 3-11(b) illustrates the device structure of solar cell subjected to encapsulation.
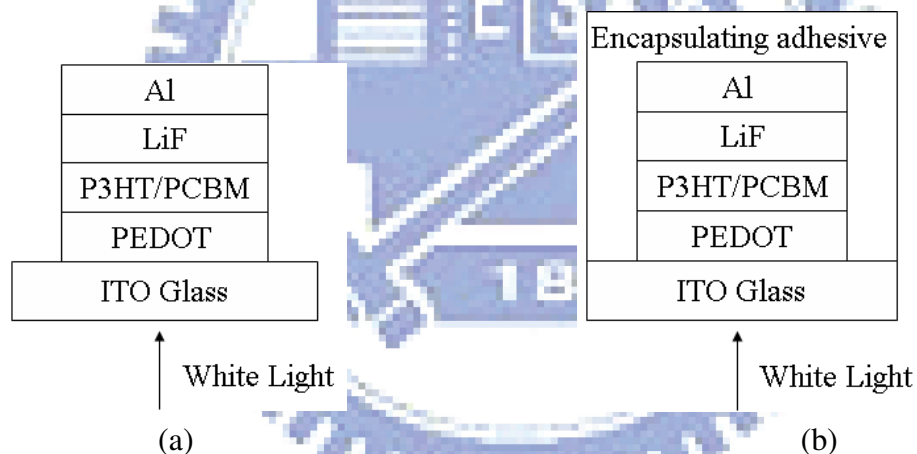
Fig. 3-11. Structures of organic solar cells (a) prior to and (b) after encapsulation. The layer thicknesses of devices are: ITO glass/PEDOT(30 nm)/P3HT:PCDM(50 nm)/LiF(10 nm)/Al(80nm).

3.2.6. Characterizations and Reliability Test of OSCs

Thermogrametric analysis (TGA), gas penetration, transmission electron micrograph (TEM), and electrical conductivity were measured by a JHS-100 TGA, a gas penetration meter (Illinois-8501), a Philips/Tecnai F20 TEM, and a 4-point

probe (Everbeing SR-4), respectively. Thermomechanic analysis (TMA), adhesion strength, and film thickness were recorded on a Seiko SSC 5000 TMA, a micro-computer universal testing machine (Hung Ta Co.) with the standard test method (ASTM D1002) and a surface profiler (TENCOR P-10), respectively. The current-voltage (I-V) curves for OSCs were measured in the air by an electric meter (Keithley 238), whose accuracy can reach picoampere, under illumination of white light from a 300 W halogen lamp (Saturn Co.) whose intensity was recorded on a radiometer (IL-1700).

3.3. Encapsulation of LEDs

3.3.1. Experimental Flow for Encapsulation of LEDs

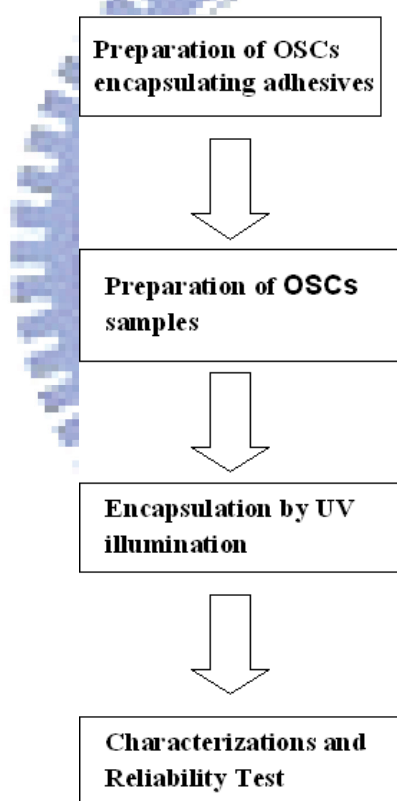The experimental flow for encapsulation of LEDs was illustrated in Fig.3-12.
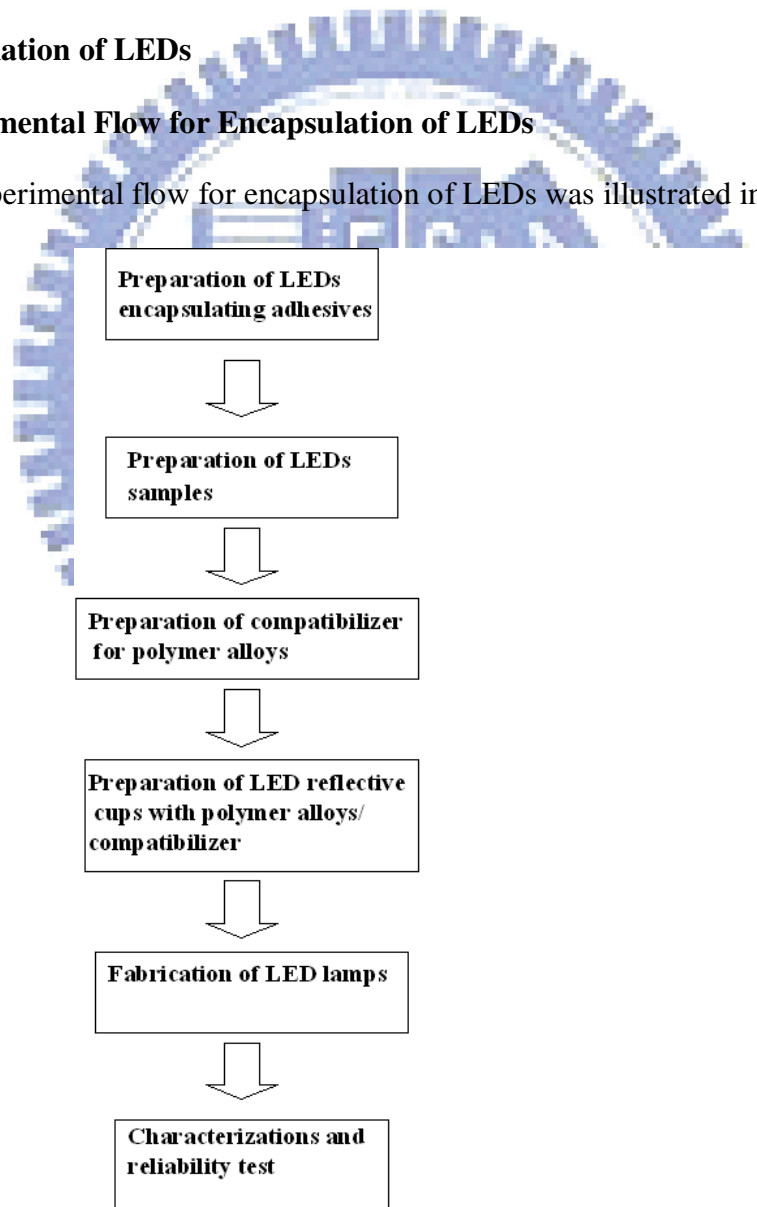
Fig. 3-12. Experimental flow for encapsulation of LEDs.

3.3.2. Materials for LED Encapsulating Nanocomposites

The chemical structure of silicone-acrylate monomer for the preparation of UV-curable LED encapsulating resins has been manifested in Fig. 3-2. All chemicals were obtained from UCB Co. and used without further purification. The inorganic fillers including silica and alumina particles with sizes = 30-100 nm were obtained from Aldrich Co.

3.3.3. Preparation of LED Encapsulating Nanocomposites

Silicone-acrylate monomer (180 g), Irgacure 651 (2 g), Darocur 1173 (1 g), Irgacure 819 (0.5 g), and alumina filler (20 g) were mixed for 30 min and then illuminated by a UV lamp (Entela UVP; wavelength = 365 nm) at the power of 100 W for 20 min (Scheme 2). The M_n, M_w, M_w/M_n ratio, and viscosity of silicone-acrylate nanocomposites were 37,300, 83,200, 2.23, and 7,200 cps, respectively.

3.3.4. Materials for LEDs Samples

The blue-light GaN chips and phosphors (yttrium aluminum garnet-$Y_3Al_5O_{12}$; YAG) for LEDs were acquired from Tekcore Co. (Taiwan) and Nichia Co., respectively. All the materials were used directly without further purification.

3.3.5. Preparation of LED Samples

The phosphor was firstly dispersed in the silicone-acrylate encapsulating nanocomposites (phosphor:silicone-acrylate nanocomposites = 12:88 in weight ratio). Then we dripped it into the bowel of lead frame which a commercial blue chip (460 nm, 0.015 in^2) was fixed on and cured it under UV illumination for 10 sec. Finally, the lead frame with blue chip and phosphor was inserted into lens. The silicone-acrylate encapsulating nanocomposite resin was full-filled into the lens and cured it by UV

illumination for 5 min to complete the preparation of LEDs samples with structure shown in Fig. 2-4.

3.3.6. Preparation of Compatibilizer for Polymer Alloys

3.3.6.1. Materials for Compatibilizers for LEDs

The LDPE pellet (NA 20766) with density = 0.923 g/cm^3 and melt index = 8 g/10 min was supplied by USI Far East Co. of Taiwan. The GMA, and PE-g-acrylic acid (PB1009), whose chemical structures were shown in Fig. 3-14, were obtained from Japanese Oil and Fat Co. and BP Performance Polymer Inc., respectively. The initiator, 2,5-dimethyl-2,5-bis(t-butyl- peroxy)hexane (TX 101) as shown in Fig. 3-13, with a half-life approximately 6 min at 160°C was purchased from the Akzo Chemie Co.
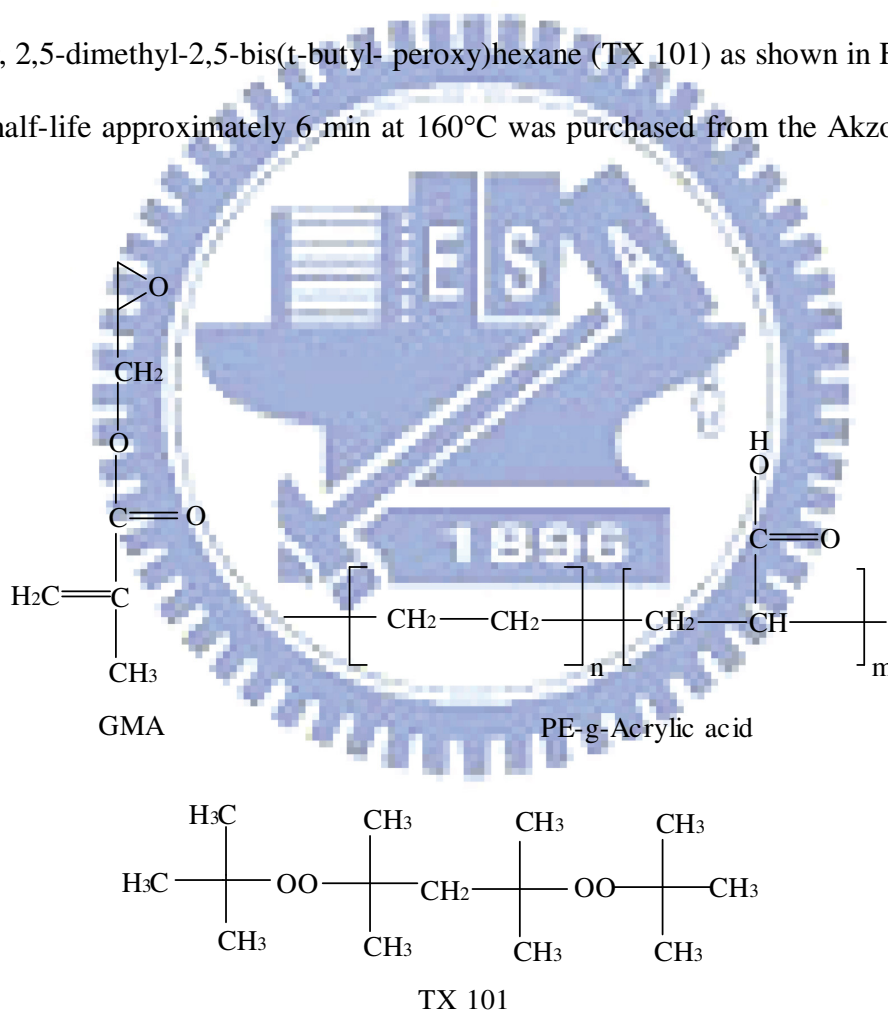
Fig. 3-13. Chemical structures of GMA, PE-g-Acrylic acid, and TX 101.

3.3.6.2. Grafting Process of GMA and LDPE for Compatibilizers

The grafting reaction was manifested in Scheme 3 and carried out by using a

twin screw extruder (W&P, ZSK 25). The LDPE pellets were fed at 40 g/min into the hopper and the GMA/TX 101 solution and were injected into the twin screw extruder from the injection nozzle via a liquid chromatography pump (Fig. 3-14). The extrudate was pelletized and then dried prior to analysis. The crude polymer was dissolved in hot toluene, precipitated the product with methanol, and then dried in a reduced pressure at 50°C for 24 hrs. The element analyzer (Heraeus CHN-0-Rapid F002) was used to analyze the contents of oxygen of the dried polymer. Thin film samples for Fourier-transform infrared (FTIR) analysis were prepared by pressing the precipitated resin between two mylar sheets at 120°C and 5 ton/cm^2 for 1 min. FTIR measurements were performed by using a Bio-Rad Digitlab Division UMA 300/FTS-40 spectrometer. The thermalgravimetric analysis (TGA) was carried out by using a Perkin-Elmer TGA7 and in temperatures ranging from room temperature to 470°C at a heating rate of 10°C/min in nitrogen ambient.

Scheme 3-3
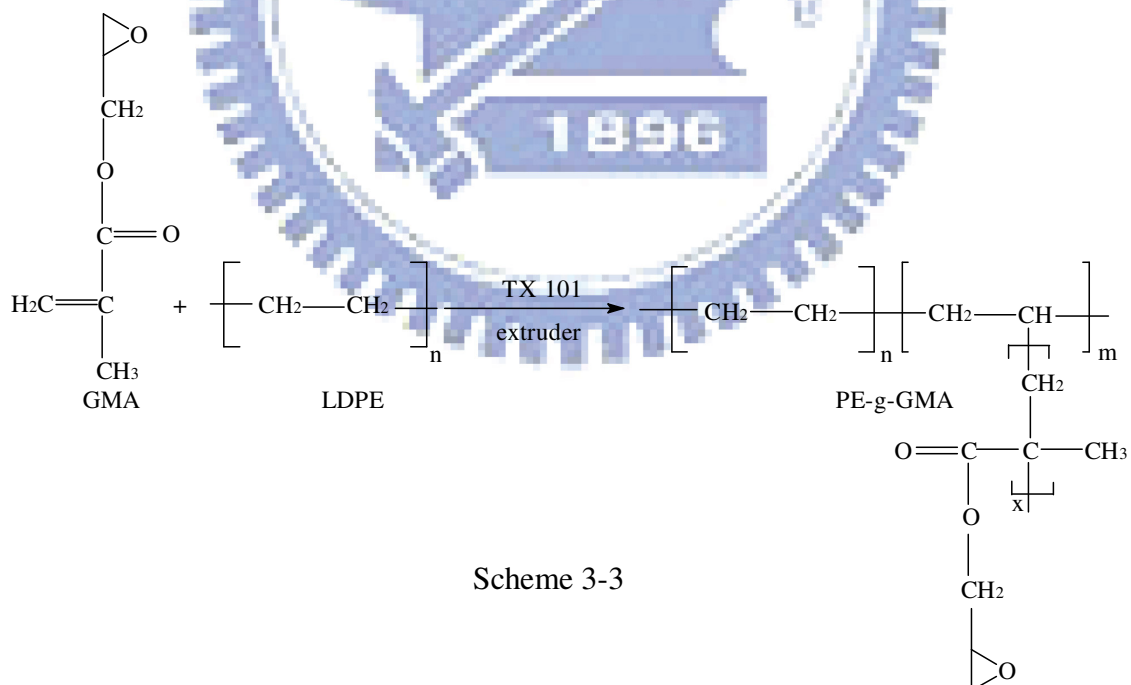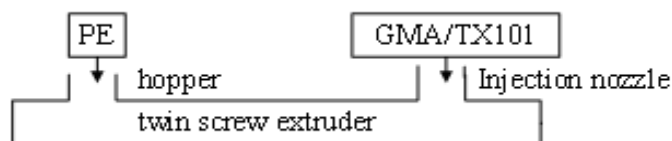
Fig. 3-14. The procedure used for the grafting reaction.

3.3.7. Preparation of LED Reflector Cups with Polymer Alloys/Compatibilizer

3.3.7.1. Materials for Polymer Alloys

The PET, PPS (P-4), and nylon 6,6, whose chemical structures were shown in Fig. 3-15, were obtained from Shinkong Synthetic Fibers Co., Du Pont Co., and Phillips Petroleum Co., respectively.
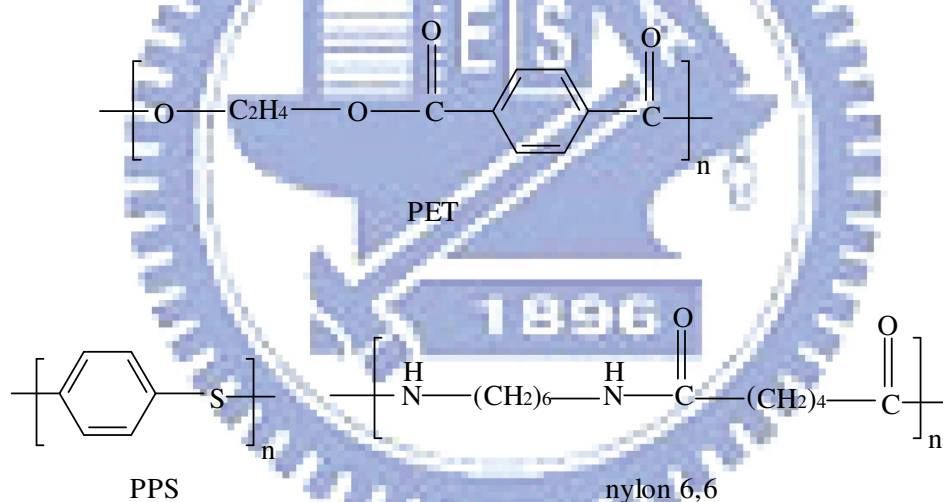
Fig. 3-15. Chemical structures of PET, PPS, and nylon 6,6.

3.3.7.2. Manufacture of LED Reflector Cups

PPS powder, PET or nylon 6,6 pellets/glass fiber, TiO_2 powder, and the PE-g-GMA compatibilizer were mixed in the twin screw extruder at 280°C at a screw speed of 300 rpm. After the extrudate was then cooled, palletized, and injection-molded, the polymeric reflector cups were manufactured as shown in Fig. 3-16.
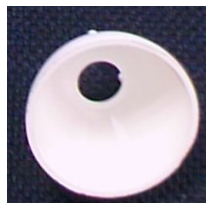
Fig. 3-16. Polymeric reflector cups for LEDs.

3.3.8. Fabrication of LED Lamps

The LEDs samples fabricated previously (see Sec. 3.3.5) were placed into the polymeric reflector cups for form the LED lamps as shown in Fig. 3-17.
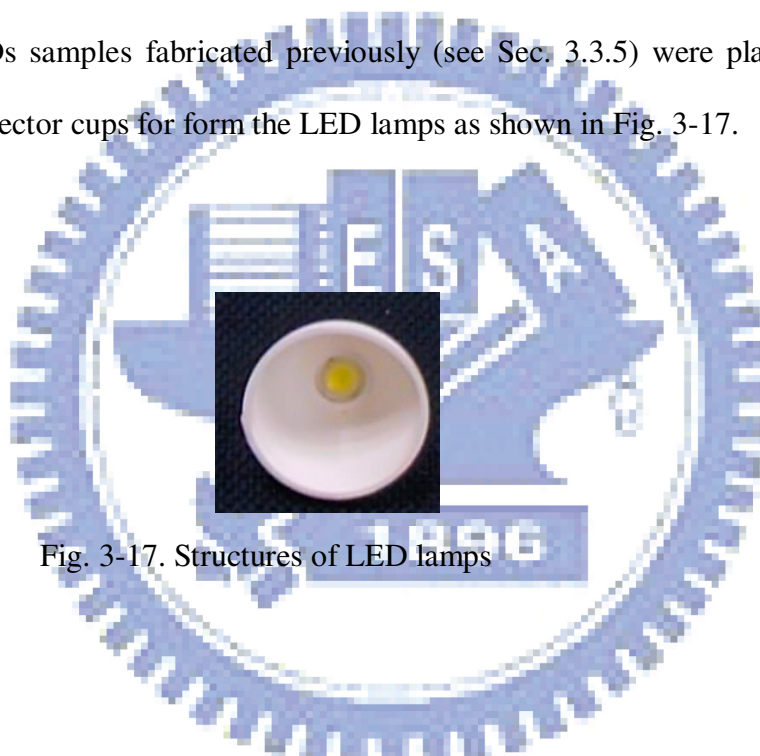
Fig. 3-17. Structures of LED lamps

3.3.9. Characterizations and Reliability Test of LEDs

We measured the viscosity and molecular weight with a viscosity meter (Viscolite 700) and a GPC (Waters Alliance GPC V200), respectively. The transparency, refractive index, and gas penetration were examined with a UV/Visible spectrometer (HITACHI U-3300), a ellipsometry (Filmetrics F20), and a gas permeation meter (Illinois-8501), respectively. The UV lamps (wavelength = 180 to 400 nm) used for synthesis and curing were Entela UVP 100W and 2450W, respectively. Moreover, the lifetimes of LEDs were recorded by lifetime-meter

(Spectrascan PR650).

Impact test specimens were prepared by an injection molding machine (Toshiba IS55). Izod impact test was conducted on unnotched specimens at 25°C according to ASTM D256 test standard. Morphologies of fractured surfaces of PPS/PET alloys were examined by scanning electron microscopy (SEM, Cambridge model S360).

Chapter 4

Results and Discussion

4.1. UV-assisted Synthetic Procedure

Ultraviolet (UV) light is the high-energy electromagnetic radiation with wavelength ranging from 180 to 400 nm. The main principle of UV-assisted synthetic procedure is to induce the dissociation of photoinitiators, generating free radicals to result in initiation, propagation and termination for photo-polymerization [15]. Scheme 3-1 and 3-2 present the UV-assisted synthetic procedure of encapsulating adhesives. In this study, the reactions of PU-acrylate and silicone-acrylate with UV-assisted synthetic procedure takes only 10-20 min, while that with conventional thermal methods takes several hours for completion. Moreover, the viscosities of PU-acrylate and silicone-acrylate prepared by UV irradiation (16,300 cps for PU-acrylate; 7,200 cps for silicone-acrylate) are larger than that prepared by conventional thermal methods (8,500 cps; reaction duration = 8 hrs for PU-acrylate and 5,300 cps; reaction duration = 20 hrs for silicone-acrylate) and no solvent is necessary in the UV-assisted synthetic procedure. These advantages fit the requirements for the low-cost and clean production of encapsulating adhesives or other polymeric materials.

Moreover, the silica and alumina particles were well dispersed in polymer matrices (Figures. 4-1 and 4-2), thus the gas penetration can be improved.
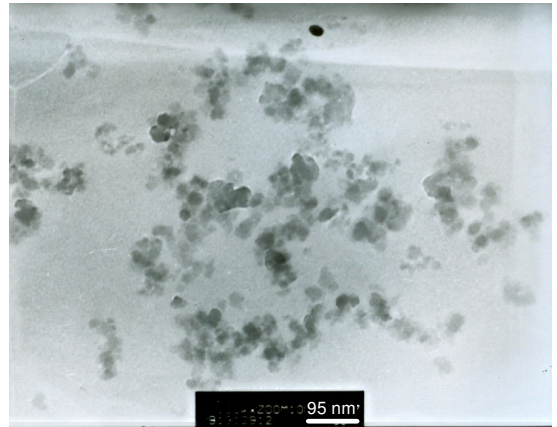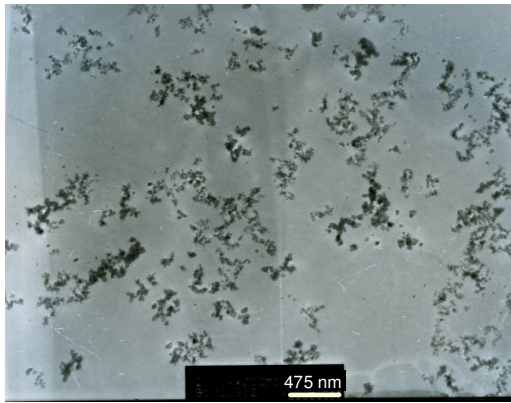
Fig.4-1. TEM micrographs of PU-acrylate/silica nanocomposites.
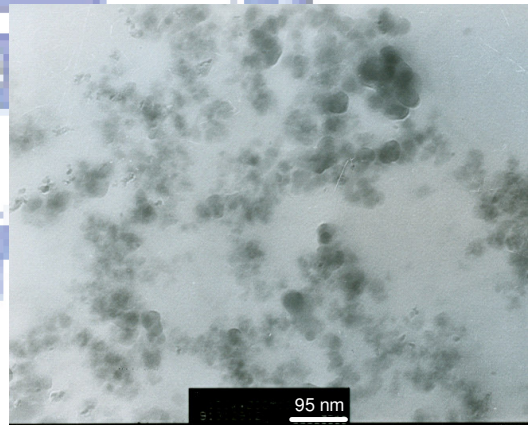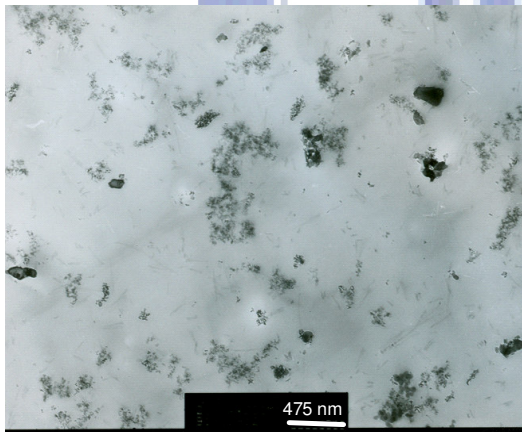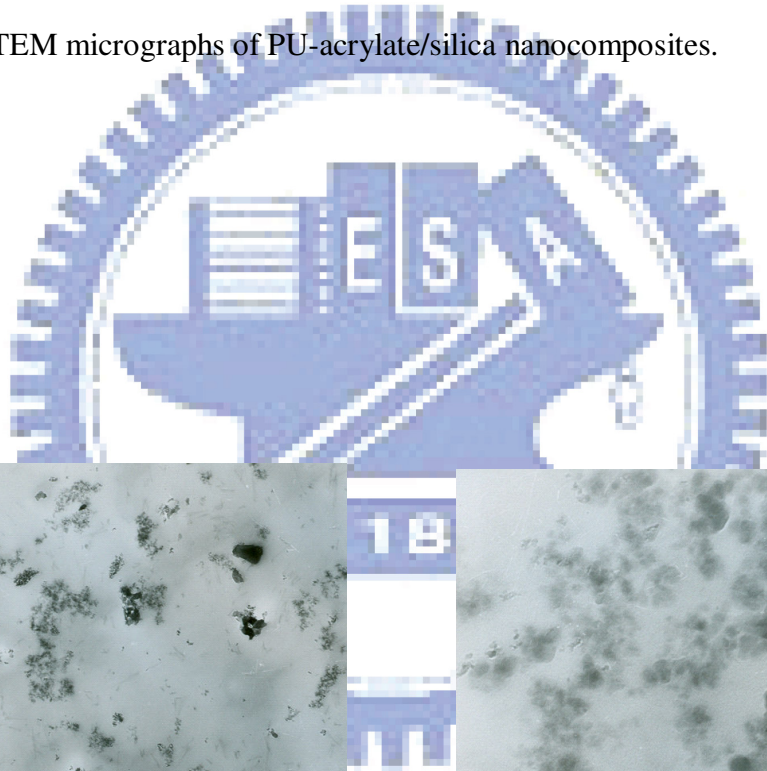
Fig.4-2. TEM micrographs of silicone-acrylate/alumina nanocomposites.

4.2. Lifetime Enhancement of OLEDs

As shown in Fig. 4-3(a), the lifetimes of OLED samples are strongly affected by the thickness of the protection layer, LiF. Without LiF, the luminance sharply drops when the device is lighted up and the half-lifetime, defined as the duration while the luminance decays from the original amount to its half, is only 4 hrs, revealing the oxygen and moisture in the air deteriorate the metal electrodes and organic layers. When LiF is deposited, however, the half-lifetime drastically rises to be 20 (LiF = 80 nm) and 31 hrs (LiF = 100 nm), respectively, representing the LiF has the resistance of the oxygen and moisture in the air and thus the lifetimes of lab-made OLEDs are prolonged. Experimental results manifest that the lifetimes of OLEDs can be modulated with the LiF thickness and the devices with thicker LiF films exhibit better barrier effects.

(a)   (b)
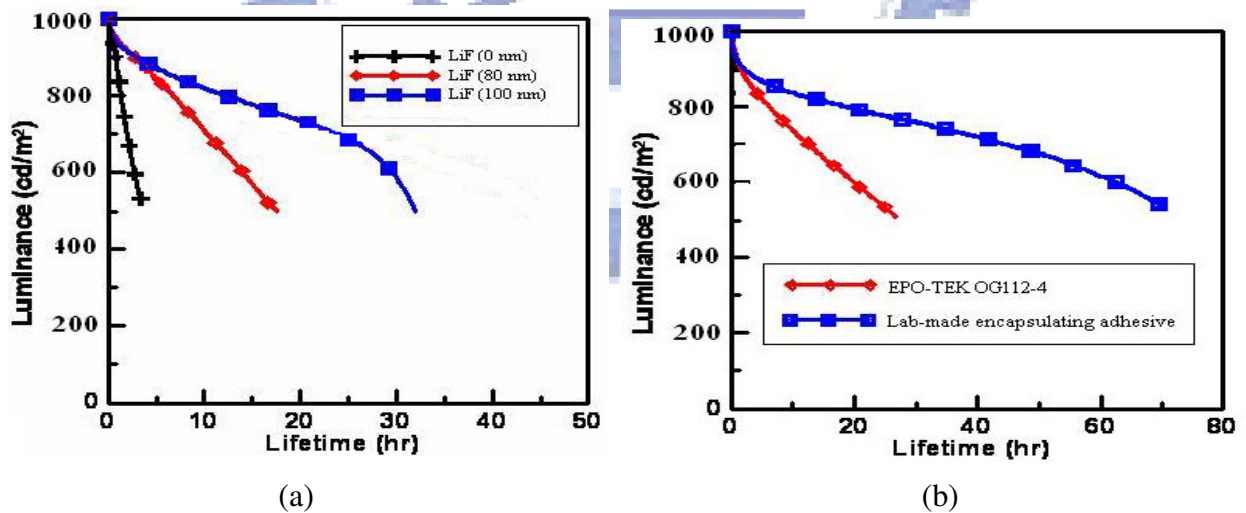
Fig.4-3. Lifetimes of lab-made OLEDs (a) Type 0 and I (b) Type II.

Although the half-lifetimes of lab-made OLEDs have been promoted to reach 31 hrs, it remains unsatisfied. In order to further improve the lifetimes, lab-made encapsulating adhesives were spin-coated in the OLED devices and cured with the UV illumination as shown in Fig. 3-6(c). The LiF layer inserted between the cathode and the encapsulating adhesives not only exhibits the gas penetration as described above but also avoids the corrosion of encapsulating adhesives (*i.e.* PU-acrylate), which are slightly acidic, on the cathode (Al layer). As shown in Fig. 4-3(b), application of encapsulating adhesives dramatically enhances the half-lifetimes of OLED devices to 72 hrs, which are 2.3 folds to those of Type I (LiF = 100 nm) and 18 folds to those without encapsulation (Type 0). This result shows that the encapsulating adhesives can further block the entry of moisture and oxygen in the air into the OLEDs, suppressing the degradation of organic materials and metal electrodes. In comparison with commercial UV curable epoxy-based encapsulating adhesives (EPO-TEK OG112-4; Epoxy technology Inc.), the nanocomposite encapsulating adhesives exhibit longer lifetimes and shorter curing duration since the half-lifetimes and curing times of EPO-TEK OG112-4 are 35 hrs and 2 min, respectively. This indicates that PU-acrylate can be an alternative polymer matrix to epoxy resins for the encapsulation of OLEDs *via* the appropriate prescription of photoinitiators and dispersion of fillers. Compared with the literature data for the lifetimes of OLEDs [40], our OLED devices with multi-layer encapsulation exhibit better gas blocking capability since the half-lifetimes of devices with packages reported in the literature are only 3.1 folds to those without packages.

Experimental results have proved that LiF and lab-made encapsulating adhesives for OLEDs encapsulation have better lifetime enhancement than other known materials because PU-acrylate exhibits better water proof propensities than other

polymers [15] and high adhesion strength with LiF [10]. Moreover, LiF has tougher chemical resistance to encapsulating adhesives than other inorganic materials [41]. Consequently, the encapsulation combining the LiF and PU-acrylate can effectively reduce the gas permeability. In the near future, synthesis of UV-curable encapsulating adhesives with different polymer matrices and fillers will be carried out in order to further improve the lifetimes of OLEDs.

4.3 Electroluminescent Properties of Color/Luminance Tunable OLEDs and Their Lifetime Enhancement with Encapsulation

4.3.1. Color Modulation and EL Effect of OLEDs with Distinct NPB/ADS082BE Layer Thicknesses

As shown in Figs. 4-4(a)-(c) as well as Fig. 4-5, the EL hue and luminance of OLED samples strongly depend on the thickness of NPB (hole transport layer) and ADS082BE (blue-color emitting layer). With the bias voltage = 7 V and the NPB thickness = 80 nm, the OLED with thinner ADS082BE (35 nm) emits blue light ($CIE_{x,y}$ = (0.18,0.27)) and that with thicker ADS082BE (50 nm) emits deep-blue light ($CIE_{x,y}$ = (0.12,0.20)). Moreover, the luminance of former (350 cd/m^2) is higher than that of the latter (10 cd/m^2). This result indicates that the device with thicker ADS082BE can effectively confine all the holes in the ADS082BE layer, whose emitting efficiency is lower, so that the recombination almost takes places in the blue-color emitting layer; however, the device with thinner ADS082BE cannot completely restrict the holes in the ADS082BE layer and some holes can overcome the energy barrier between the ADS082BE and Alq$_3$ layers as shown in Fig. 4-6(a) [42] so that a small portion of recombination occurs in the green-color emitting layer

(Alq$_3$), whose emitting efficiency is higher, inducing the red-shift of EL color and strong luminance.

When the layer thickness of NPB was reduced to be 50 nm, nevertheless, the OLED with thinner ADS082BE (35 nm), which is lighted up at 7 V, irradiates blue-green light (CIE$_{x,y}$ = (0.23,0.30)), revealing the decrease for electrical resistance of NPB can further increase the mobility of hole and raise the possibility of the recombination in the Alq$_3$ layer. In addition, its luminance (450 cd/m^2) at 7 V is highest among Device III due to its lowest electrical resistance. Since the EL efficiencies of NPB as well as ADS082BE are diverse and the location of recombination can be manipulated by the layer thickness of NPB/ADS082BE, the color/luminance tunable OLEDs can thus be fabricated.
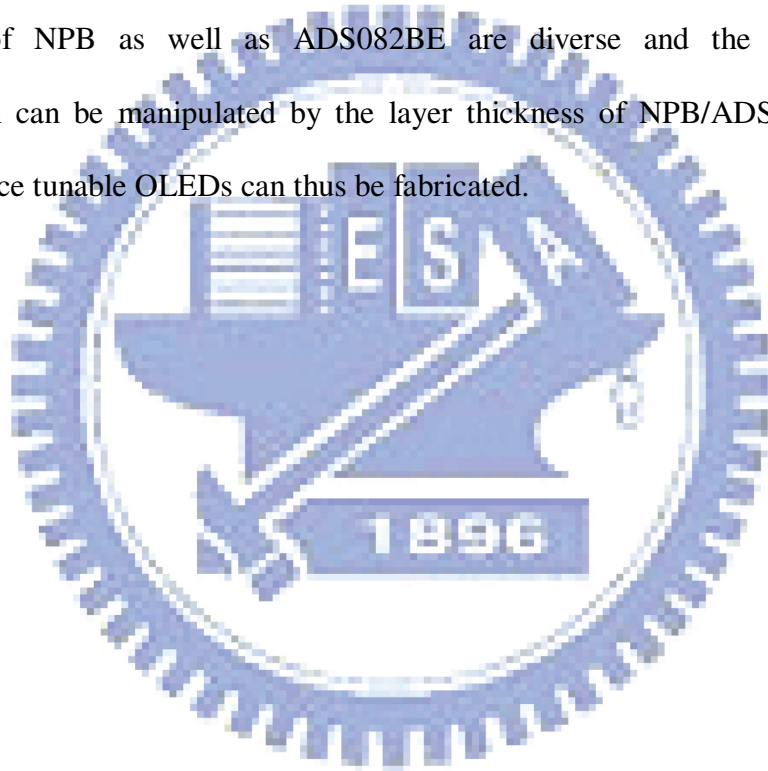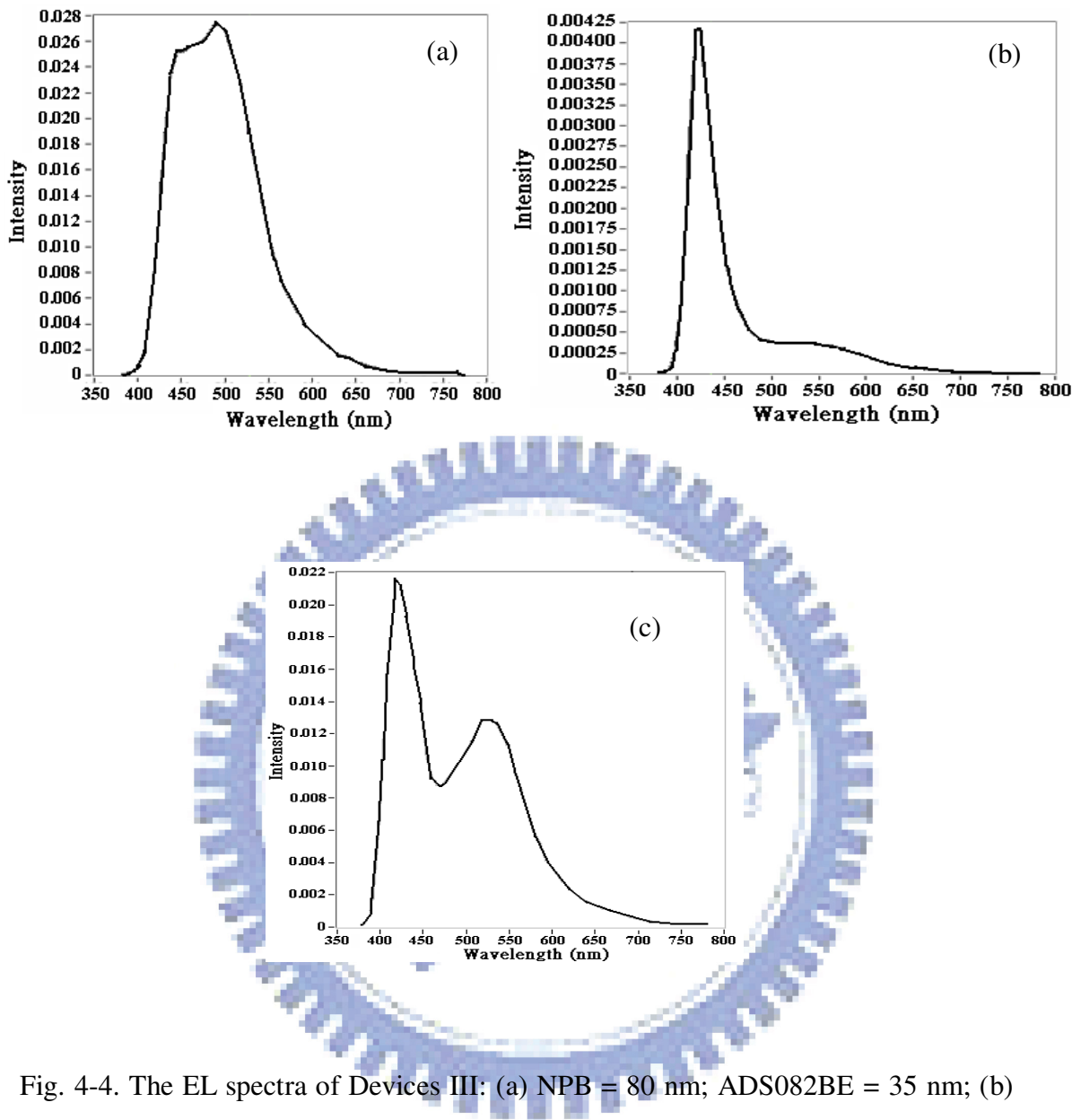
Fig. 4-4. The EL spectra of Devices III: (a) NPB = 80 nm; ADS082BE = 35 nm; (b)

NPB = 80 nm; ADS082BE = 50 nm; (c) NPB = 50 nm; ADS082BE = 35

nm.
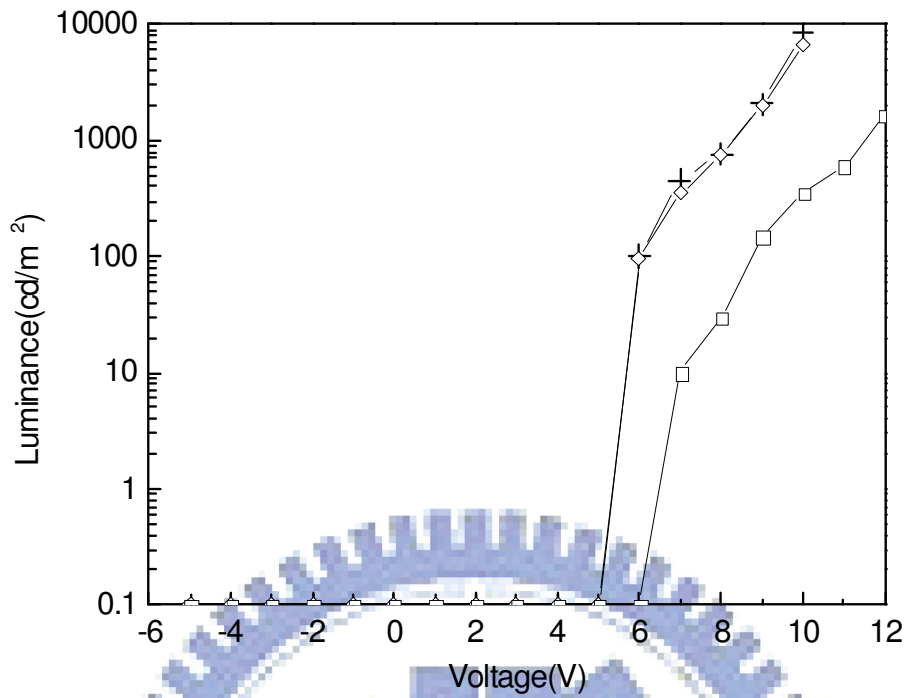
Fig. 4-5. Electroluminescent properties of Devices I (+:NPB = 50 nm; ADS082BE = 35 nm; ◇:NPB = 80 nm; ADS082BE = 35 nm; □:NPB = 80 nm; ADS082BE = 50 nm)

(a)   (b)
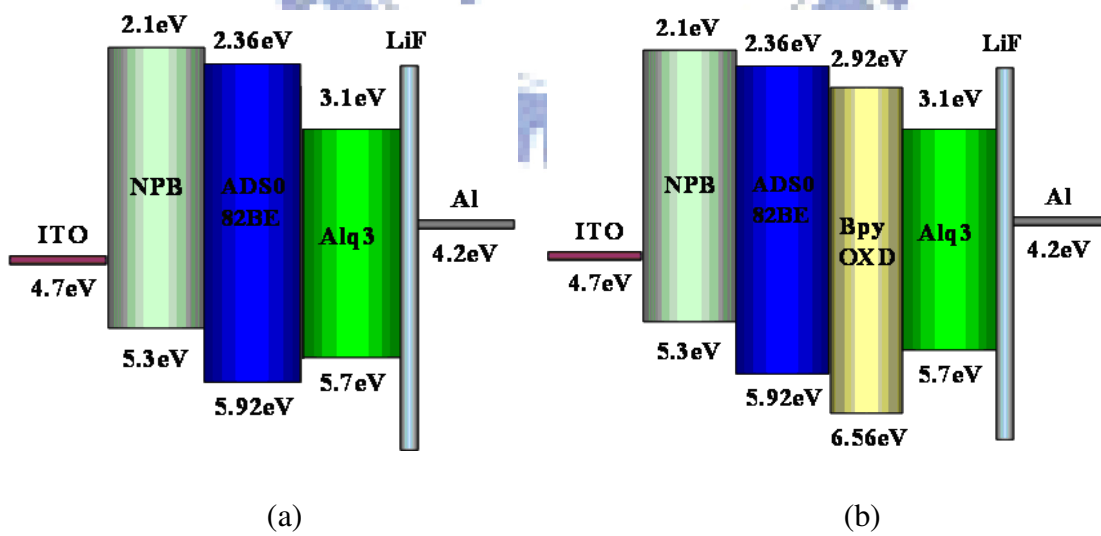
Fig. 4-6. The energy level diagrams for (a) Devices III and (b) Devices IV.

4.3.2. Introduction of Electron Blocking Layer

In order to promote the EL properties of blue-light OLEDs (*i.e*., Device III containing 80 nm NPB and 35 nm ADS082BE), Bpy-OXD (the electron blocking layer) was introduced into the device. Without Bpy-OXD, the electron can freely arrive at either ADS082BE or Alq$_3$ layer and the recombination occurs when the hole and electron meet as shown in Fig. 4-6(a). With Bpy-OXD, however, the hole can be impeded in the boundary of Bpy-OXD/Alq$_3$ since it cannot overcome the energy barrier between the Bpy-OXD and Alq$_3$ as shown in Fig. 4-6(b) [43] and the recombination consequently takes place in the Alq$_3$ layer, whose emitting efficiency is higher, irradiating strong luminance. As shown in Fig. 4-7, introduction of Bpy-OXD can drastically not only raise the luminance but also lower the turn-on voltage to 3V, whereas the turn-on voltage of the OLED without Bpy-OXD is 5V. This illustrates that Bpy-OXD may hinder the entry of holes into the Alq$_3$ layer and the recombination readily occurs while electrons arrive at Alq$_3$/Bpy-OXD boundary, decreasing turn-on voltage. Despite of the addition of Bpy-OXD into OLEDs may heighten the EL intensity, the OLED with 30-nm thick Bpy-OXD exhibits weaker luminance (60 cd/m^2 at 4 V; 650 cd/m^2 at 7 V) than that with 20-nm thick Bpy-OXD (200 cd/m^2 at 4 V; 1550 cd/m^2 at 7 V). This result comes from that the hole may be trapped in the Bpy-OXD layer while the layer thickness of Bpy-OXD is larger than 20 nm, causing the electrical resistance is high enough to obstruct the migration of the hole and lessen the recombination in the Alq$_3$ layer.

Furthermore, we observed the voltage-dependent EL effect in Device IV containing 20-nm thick Bpy-OXD. As shown in Fig. 4-8 and Table 4-1, the EL spectra of OLEDs fluctuate with the applied potential and their emitting colors also vary accordingly in the range of 4 to 9 V, manifesting that the migration speed of electrons

may accelerate and the recombination zone gradually locates in the ADS082BE layer (blue emitting layer) when the applied voltage is increased. This induces the change of EL hue from deep green to light blue.
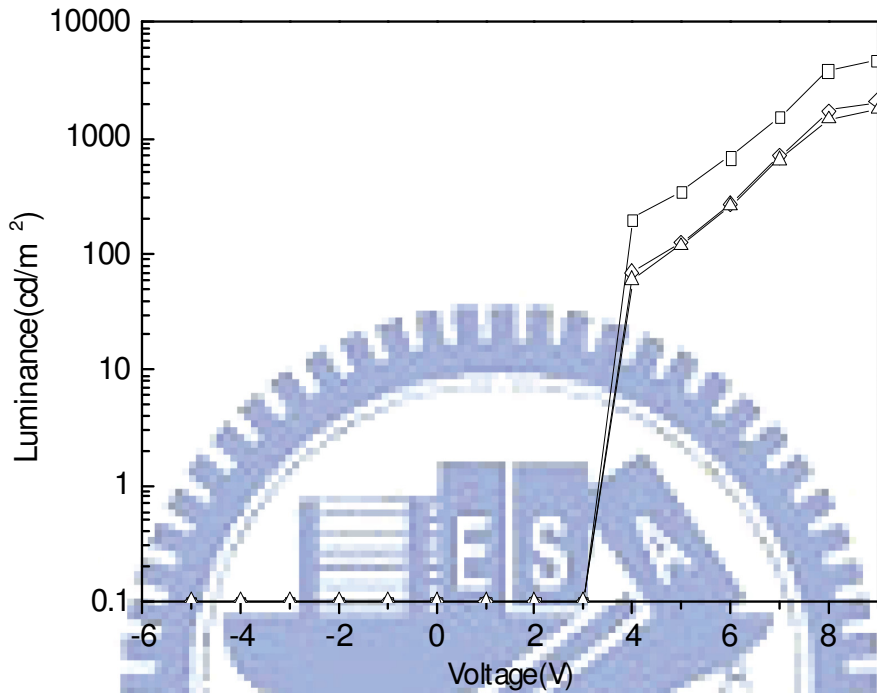
Fig. 4-7. Electroluminescent properties of Device IV ($\diamond$:Bpy-OXD = 10 nm; $\square$:Bpy-OXD = 20 nm; $\triangle$: Bpy-OXD = 30 nm).
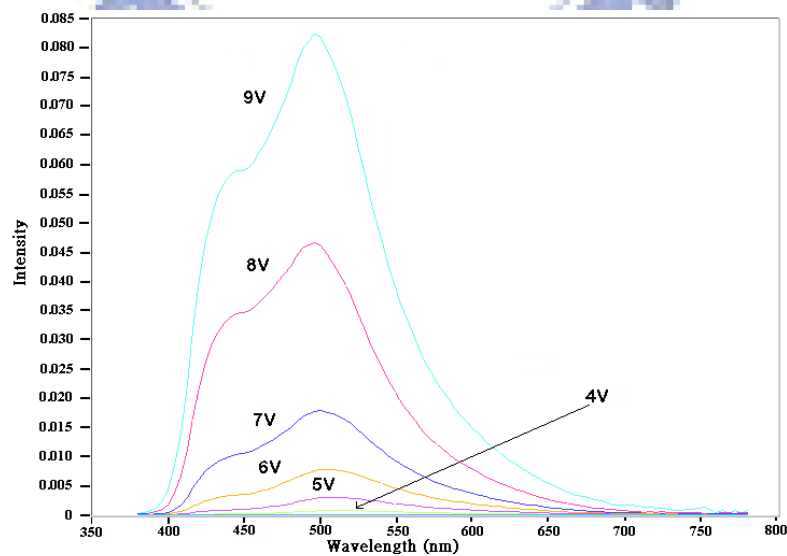
Fig. 4-8. EL spectra of Device IV with Bpy-OXD thickness = 20 nm at 4-9 V.

Table 4-1. The voltage-dependent EL properties of Devices IV with Bpy-OXD

thickness = 20 nm.

Applied voltage (V)	$CIE_{x,y}$	Luminance (cd/m^2)	EL color
4	(0.30, 0.55)	200	Deep green
5	(0.28, 0.50)	350	Green
6	(0.26, 0.46)	700	Light green
7	(0.24, 0.40)	1550	Green-blue
8	(0.22, 0.34)	3900	Blue-green
9	(0.20, 0.30)	4850	Light blue

Although the modulation of EL colors for OLEDs can be executed by the modification of light-emitting materials, the process for the tune of colors by the variation of layer thickness, introduction of electron blocking layer and manipulation of applied voltage is relatively ease, cheap, and convenient. Nonetheless, as shown in Fig. 4-9, the luminance drastically decreases when Device IV (NPB = 80 nm; ADS082BE = 35 nm; Bpy-OXD thickness = 20 nm) without encapsulation is actuated at 7 V and the half-lifetime is only 9 hrs, representing the moisture and oxygen in the ambient lead to the corrosion of organic layers and Al electrode. To further improve the lifetimes of OLEDs, we synthesized the encapsulating resin with high gas barrier capability and applied it for the package of lab-made OLEDs.
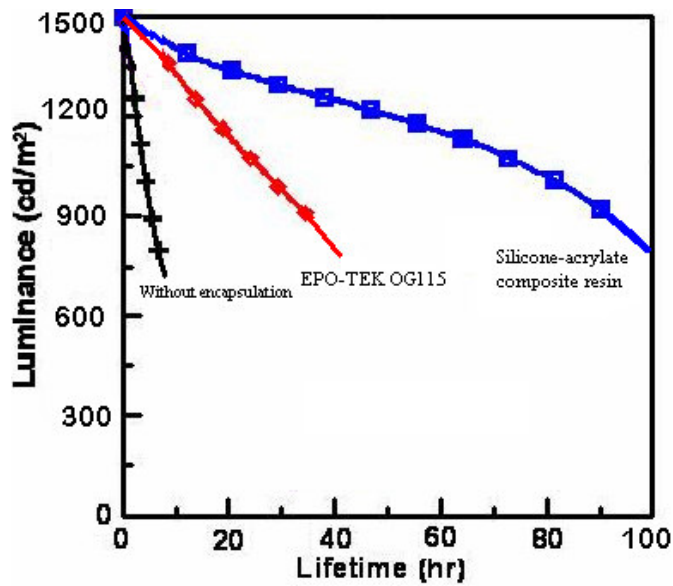
Fig. 4-9. Lifetime curves for Device IV at room temperature without encapsulation and with the encapsulation of EPO-TEK OG115 as well as lab-made silicone-acrylate composite resin at 7 V.

4.3.3. UV-curable Encapsulating Resin and Its Application for Lifetime Enhancement of OLEDs

In recent years, lifetime improvements of OLED packages with cover glass [28,29] or organic/inorganic multilayer (*e.g.*, Barix technique developed by Vitex Systems Co., *etc.*) [37] have been reported. Although the gas blocking performances of cover glass and organic/inorganic multilayer are good, their encapsulation procedures are high-cost and complicated. Consequently, a package of OLEDs with the low-cost UV-curable composite adhesive comprised of silicone-acrylate polymeric matrix and alumina inorganic filler is developed in this work.

44

Figure 4-9 shows the lifetime measurement of Device IV without encapsulation and with the encapsulation of EPO-TEK OG115 (Epoxy technology Inc.) as well as the silicone-acrylate composite resin at room temperature. Furthermore, all the luminance measurements *versus* time were carried out in a non-stop manner at constant voltage (7 V). The half-lifetimes of OLEDs with silicone-acrylate composite resin is substantially improved to 98 hrs in comparison with 9 hrs for that without package, showing that the silicone-acrylate composite resin can effectively restrict the permeation of moisture and oxygen in the air into the devices. The gas resistance of silicone-acrylate composite resin suppresses the degradation of Al electrode as well as organic materials and eventually increases the lifetimes. Compared with the commercial packaging adhesive (EPO-TEK OG115), the silicone-acrylate composite resin exhibits better gas barrier capability and shorter curing time because the half-lifetimes and curing time of OLEDs with EPO-TEK OG115 are 41 hrs and 5 min, respectively. Experimental results manifest that the composite sealing resin, which consists of silicone-acrylate matrix, finely dispersed alumina fillers and proper prescription of photoinitiators, possesses good gas barrier property than the commercial available epoxy resins-based materials.
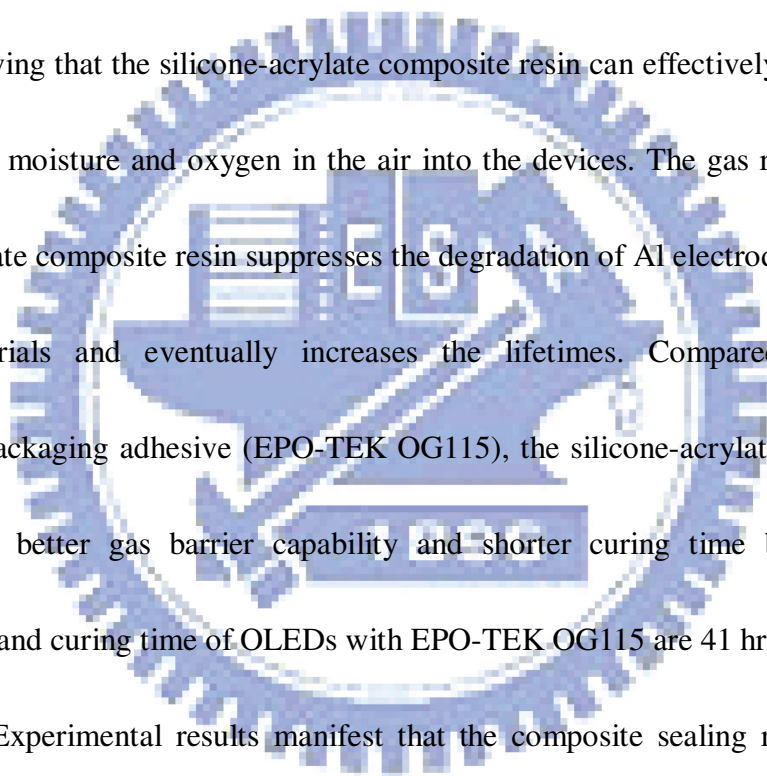
4.4. Encapsulation of OSCs

4.4.1. Polymer Matrices of Encapsulation Resins

Although 1,6-hexanedol diacrylate exhibits good mechanic properties, low brittleness after curing, and short curing time, it possesses weak thermal stability, low viscosity and high contraction after UV curing. In contrast, 3,4-epoxycyclohexane carboxylode is a superior cycloaliphatic epoxy resin with high thermal resistance, good transparency, low dimension change and moderate viscosity. In addition, the cycloaliphatic epoxy resin has lower chloride content than other epoxy resins because it is synthesized by peroxidation rather than by the reaction of hydroxyl group and epichlorohydrin [10]. The chloride ion may cause the erosion of the electronic devices in humidity. Therefore, we blended 3,4-epoxycyclohexane carboxylode with the acrylics resin to heighten the thermal resistance, diminish the shrinkage and increase the viscosity.
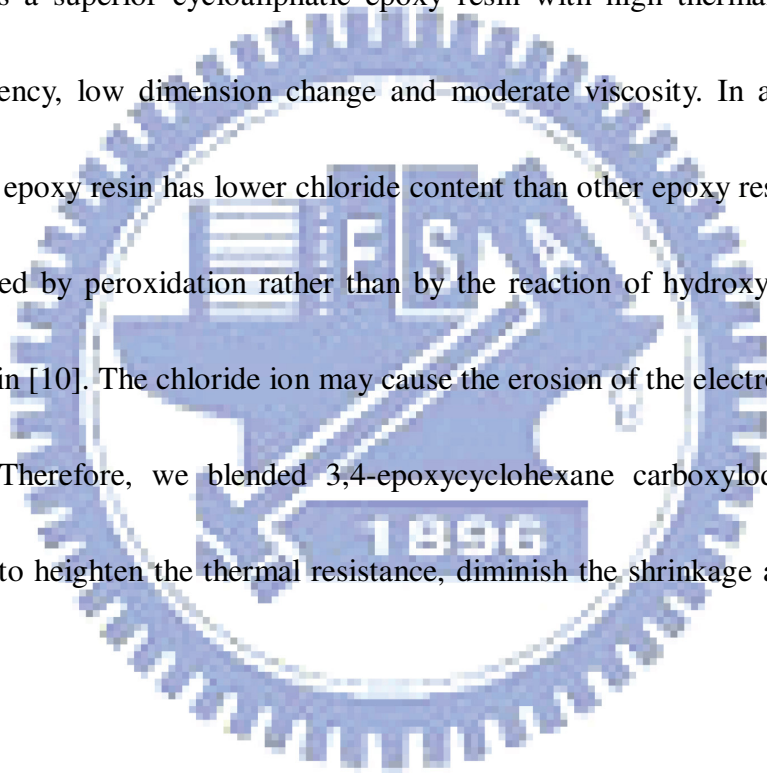
4.4.2. Thermal Characterization, Gas Barrier Properties, and Electrical Conductivities of Epoxy-Acrylate Nanocomposites

TGA characterization of epoxy-acrylate nanocomposites was executed in air and the result is depicted in Fig. 4-10. Their decomposition temperatures (T_d; at 5%

weight loss) are tabulated in Table 4-2, revealing they have excellent thermal stabilty

since all T_d's are higher than 300°C. This is very crucial on the encapsulation of the

electronic device because they can endure high temperature and resist the penetration

of gas despite the electronic device liberates much heat when actuated.
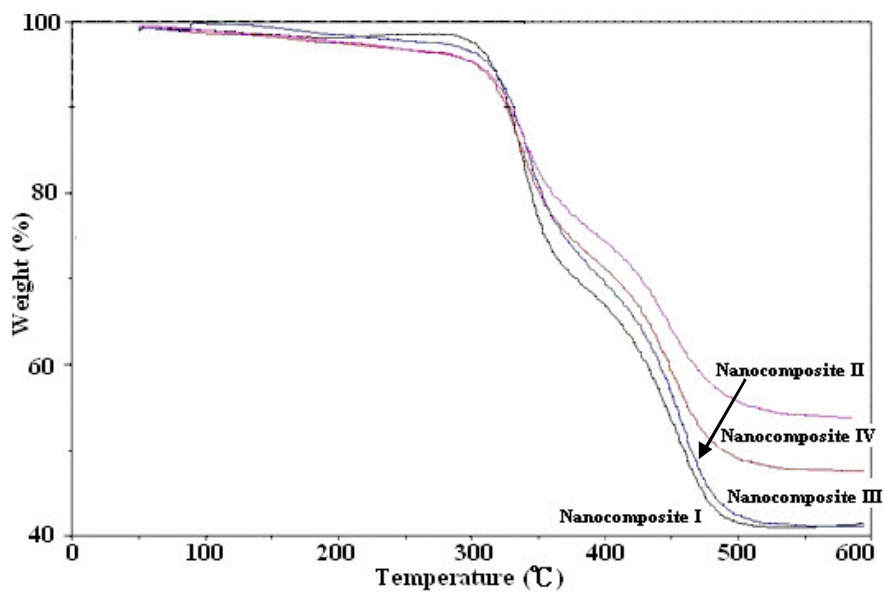
Fig. 4-10. TGA profiles of epoxy-acrylate nanocomposite resins in air.

Table 4-2. Physical properties of Epoxy-Acrylate nanocomposites.

Sample	T_d (°C)	Adhesion strength (kgf/cm^2)	Gas penetration (%)	Electrical conductivity (S/cm)
Nanocomposite I	345	117.5	10.71	1.5×10^{-12}
Nanocomposite II	340	107.4	8.17	2.3×10^{-10}
Nanocomposite III	328	90.7	7.34	4.7×10^{-10}
Nanocomposite IV	335	87.3	5.12	6.8×10^{-10}

The organic/inorganic nanocomposites exhibit good gas resistance and the introduction of Invar drastically promotes the gas barrier effect as shown in Table 2. Moreover, the gas peneration decreases with the increase of Invar because the polymer matrices/nano-silica were well dispersed (Fig. 4-11(a)) and the metal alloys lying on the polymer matrices/nano-silica may further fill in the vacancy of the polymer matrices/nano-silica and thus the gas penetration can be improved (Figs. 4-11(b)-(d)).
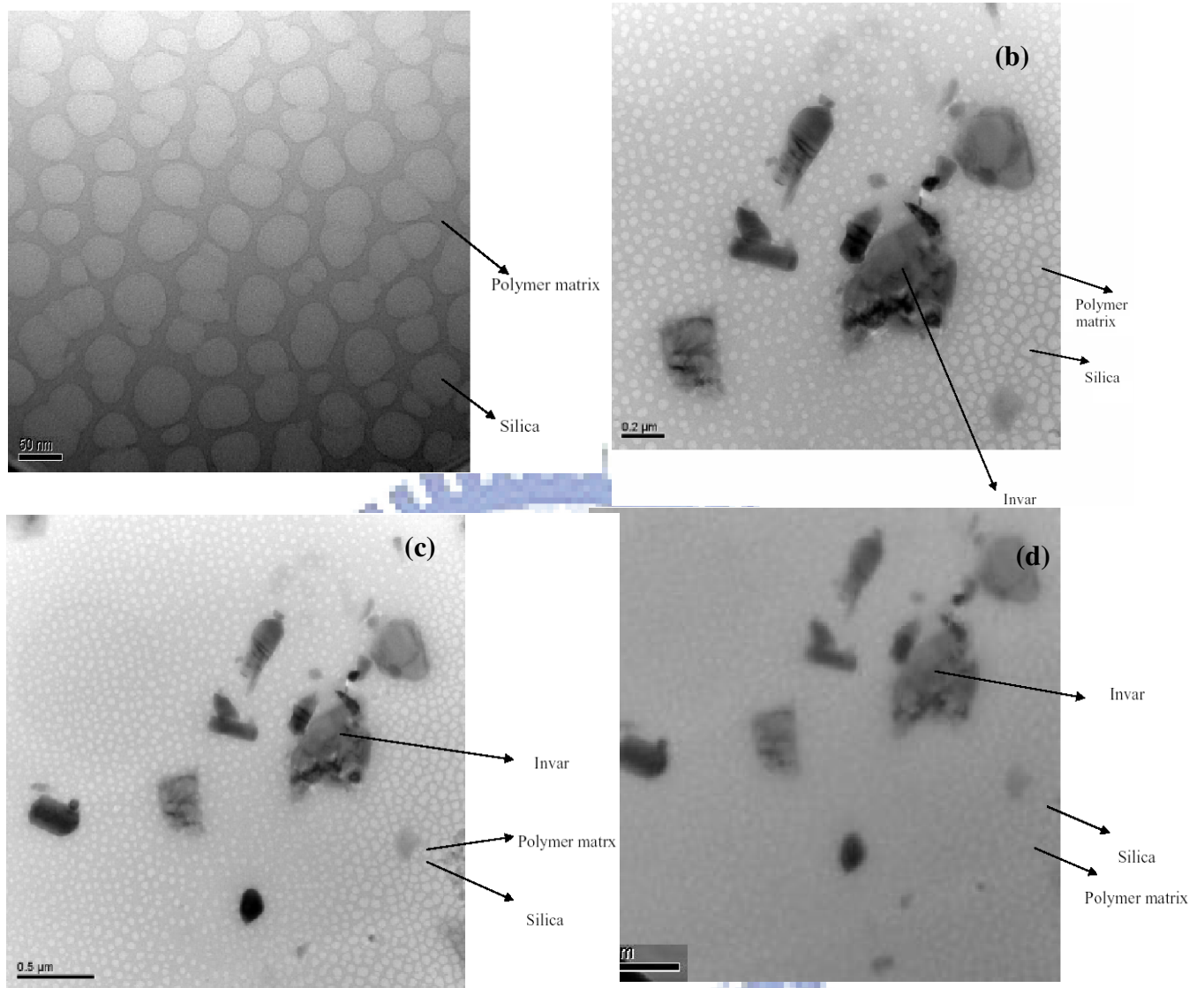
Fig. 4-11. TEM micrographs of nanocomposites(a) ploymer matrices/nano-silica,

(b),(c),(d) ploymer matrices/nano-silica/invar

We also have investigated the electrical conductivities of the nanocomposites

with a 4-point probe. Although up to 15 *wt*.% of the metal alloy (Invar) was blended

in the resins, no significant increase of electrical conductivities was observed in all

samples as shown in Table 4-2. The electrical insulation is essential to avoid electrical

interference when the device is actuated.

4.4.3. TMA Properties and Adhesion Strength of Epoxy-Acrylate Nanocomposites

As shown in Table 4-2 and Fig. 4-12, addition of Invar not only enhances the gas

barrier capability but also reduces the shrinkage. Furthermore, the dimension change

in planar direction decreases with the increase of Invar as shown in the TMA profiles

of Fig. 4-12. Nevertheless, the adhesion strength drops with the raising of Invar owing

to the poor adhesion between metal with the glass.
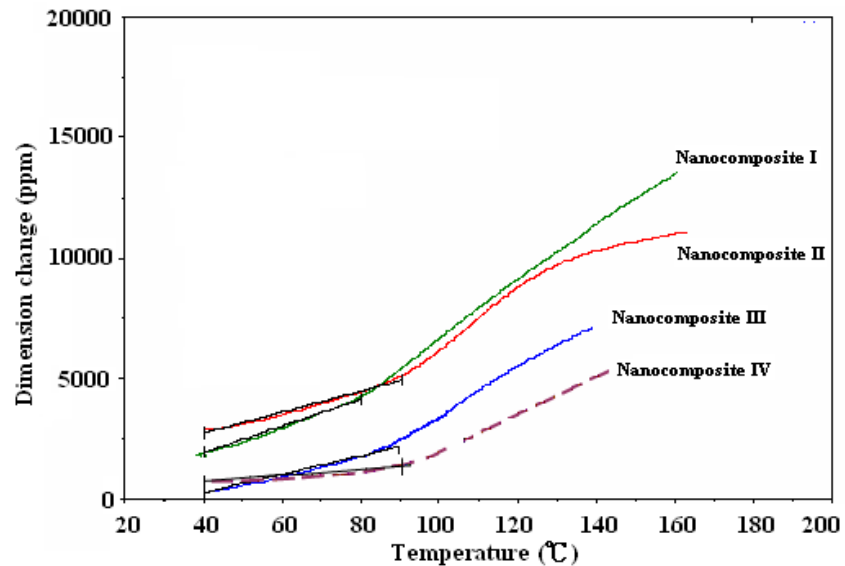
Fig. 4-12. TMA profiles of epoxy-acrylate nanocomposites.

4.4.4. Lifetime Improvements of OSCs

As shown in Fig. 4-13(a) and Table 4-3, OSC sample without encapsulation

exhibits the photoelectric conversion properties initially and its efficiency is 0.42 %. As the actuating time proceeds, nonetheless, the photoelectric conversion capability gradually decays. This is ascribed to the invasion of moisture and oxygen in the atmosphere into the device, causing the corrosion of organic materials and metal electrode. After actuating for 48 hrs, the efficiency reduces to 0.016% with a decay ratio = 96.2 %.

In order to improve the lifetime of OSCs, we applied nanocomposites IV for the device package. With the encapsulation, as manifested in the Fig. 4-13(b) and Table 4-3, the decay ratio sharply improves and is only 13 and 37% when the actuating time are 15 and 48 hrs, respectively. The result indicates that nanocomposites IV is capable of resisting the penetration of oxygen as well as moisture in the air into the device, effectively prolonging the lifetime of OSCs. Similar result can also be observed in the case of commercial encapsulating adhesive (EPO-TEK 301, Epoxy Technology Co.) as shown in Fig. 4-13(c) and Table 4-3. Compared with the photoelectric conversion properties of organic solar cells with EPO-TEK 301, the decay ratio of the device with the package of nanocomposites IV is lower, revealing that the nanocomposites IV exhibits better gas barrier capability than EPO-TEK 301.
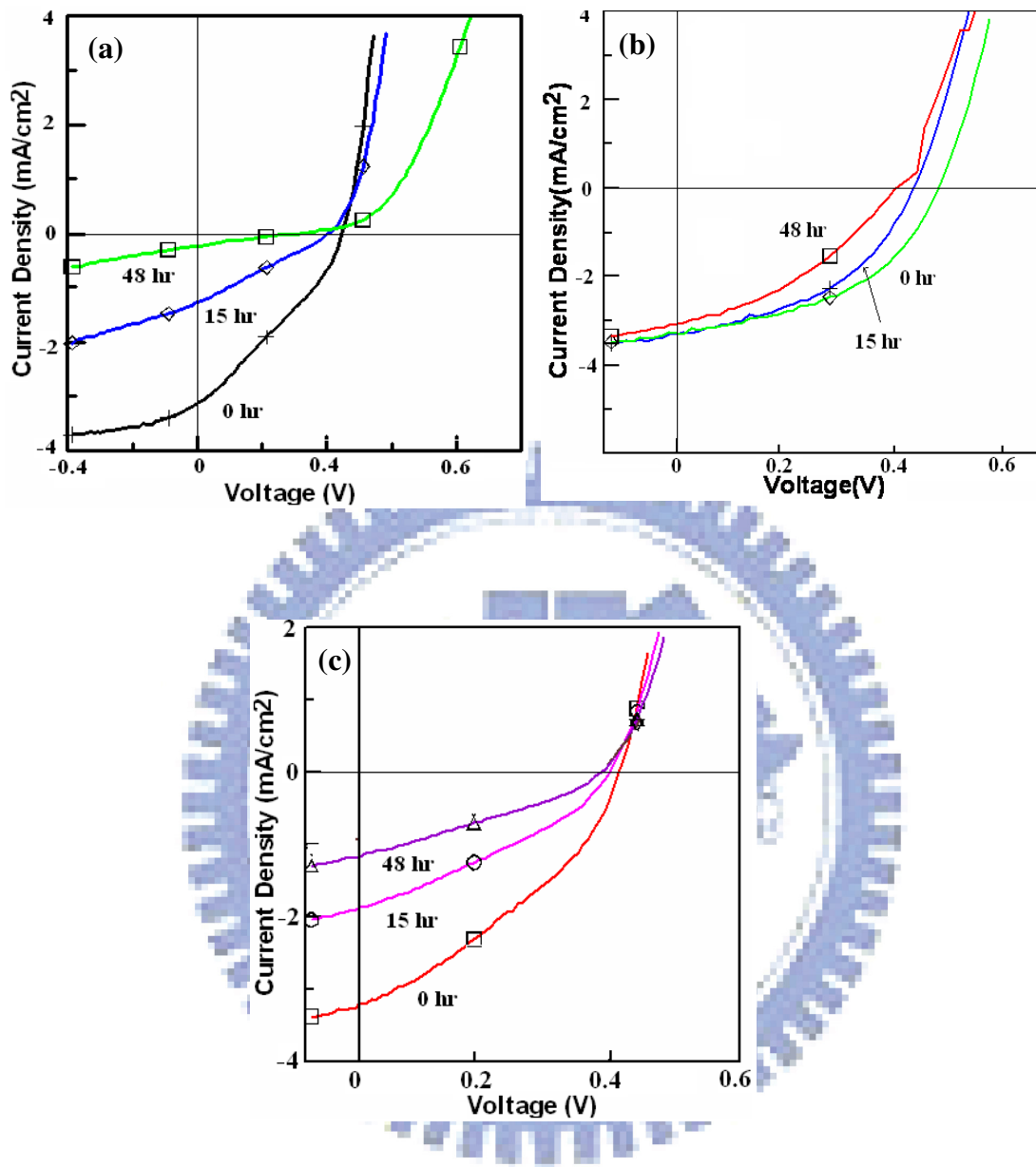
Fig. 4-13. *I-V* curves of OSC samples (a) without encapsulation (b) with

nanocomposites IV and (c) with EPO-TEK 301.

Table 4-3. Photoelectric conversion properties of OSCs without encapsulation and

encapsulated by various types of resins.

Encapsulating Material	Actuating time (hrs)	V_{OC}[a] (V)	I_{SC}[b] (mA/cm²)	FF[c] (%)	$Eff.$[d] (%)	DR[e] (%)
No encapsulation	0	0.44	3.13	31.6	0.42	---
	15	0.40	1.28	25.5	0.13	69.0
	48	0.30	0.22	23.1	0.016	96.2
Nanocomposite IV	0	0.44	3.33	48.1	0.54	---
	15	0.42	3.30	44.9	0.47	13.0
	48	0.40	3.05	37.2	0.34	37.0
EPO-TEK 301	0	0.44	3.18	34.6	0.52	---
	15	0.40	1.88	33.4	0.28	46.2
	48	0.38	0.92	28.5	0.11	78.8

[a]Open circuit voltage (V_{OC}) is defined as the voltage when the current density is zero.

[b]Short circuit current (I_{SC}) is defined as the current density when the voltage is zero.

[c]Fill factor (FF) is defined as $FF = \dfrac{VI_{max}}{V_{OC}I_{SC}}$.

[d]Efficiency ($Eff.$) is defined as $Eff. = \dfrac{V_{OC}I_{SC}FF}{P_{in}} \times 100\%$ where P_{in} is the power

intensity of white light source.

[e]Decay ratio (DR) is defined as $DR = \dfrac{(Eff_o - Eff_e)}{Eff_o} \times 100\%$ where Eff_o and Eff_e

represent the efficiency of OSC for original state (actuating time = 0 hr) and
experimental state (actuating time = 15 or 48 hrs), respectively.

4.5. Encapsulation of LEDs

4.5.1. Mechanism of Grafting Reactions for Compatibilizers

Figure 4-14 depicts the possible reactions taking place during grafting procedure [44]. First, the primary $R^\bullet$ radical produced by thermal decomposition of TX 101 extracts a hydrogen atom from PE chains (reaction (1)). The radicals generated by peroxide decomposition then attack PE, preferentially at branch chain, to produce $PE^\bullet$, which either undergo crosslinking or disproportionation (reaction (2)). Simultaneously, the homopolymerization of GMA occurs, yielding $(GMA)n^\bullet$ which undergoes chain transfer to form $PE^\bullet$ (reactions (3) and (4)). These reactive sites of PE backbone either react with GMA or capture $(GMA)n^\bullet$, and finally result in grafting reactions (reactions (5) and (6)). Among these possible reactions, reaction (5) is the key reaction for the grafting process of LDPE and GMA.

$$\boxed{PE}-H + R\cdot \longrightarrow \boxed{PE}\cdot + RH \qquad (1)$$

$$\boxed{PE}\cdot + \boxed{PE}\cdot \longrightarrow \begin{array}{c}\boxed{PE}\\\boxed{PE}\end{array} + \begin{array}{c}\boxed{PE}=CH2\\\boxed{PE}-H\end{array} \qquad (2)$$

$$GMA \xrightarrow{\; R\cdot \;} (GMA)n\cdot \qquad (3)$$

$$(GMA)n\cdot + H-\boxed{PE} \longrightarrow (GMA)n + \boxed{PE}\cdot \qquad (4)$$

$$\boxed{PE}\cdot + GMA \longrightarrow \boxed{PE}-GMA\cdot \xrightarrow{\; GMA \;} PE\text{-}g\text{-}GMA \qquad (5)$$

$$\boxed{PE}\cdot + (GMA)n\cdot \xrightarrow{\; GMA \;} PE\text{-}g\text{-}GMA \qquad (6)$$
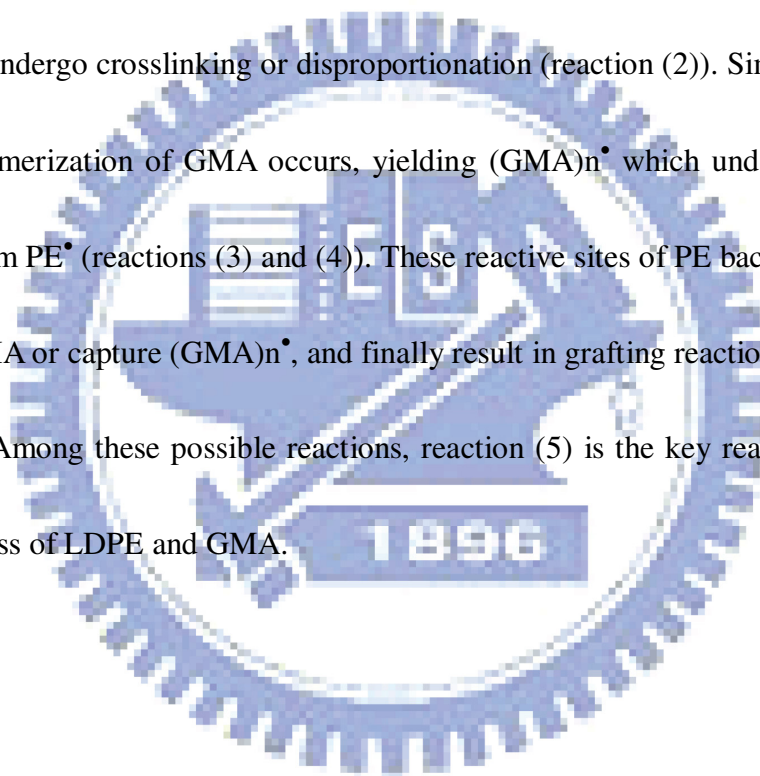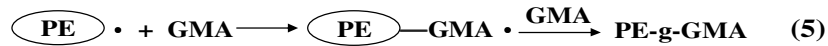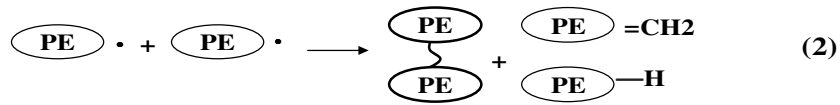
Fig. 4-14. Overview of the free radical reactions.

4.5.2 .The Different Types of Grafting Procedure

Fig. 4-15 shows the dramatic influence of grafting procedure on the gel content of the PE-g-GMA. The gel contents of the grafting reaction for the three different types of reaction processes are compared at the same composition and conditions.

It is found that the gel content of the grafting reaction varies as:

Process 2(67.5%)>Process 3(22.0%)>Process 1(1.85%) It indicates that higher gel content is obtained as the PE$^\bullet$ forms earlier (such as Process 2). However, the gel content is lowered as the (GMA)n$^\bullet$ are generated before the occurrence of PE$^\bullet$ (such as Process 1). On the other hand, the gel content of Process 3 is between that of the Process 1 and Process 2 when the PE$^\bullet$ and (GMA)n$^\bullet$ are generated in competition during the period of grafting reaction.

For the process 2 in Fig. 4-15, the amount of crosslinked polymer is considerable

because the reactions (1) and (2) are dominant. For the process 1 in Fig. 4-15, the (GMA)n$^\bullet$ are generated first. Then, the grafting reaction will be initiated by the (GMA)n$^\bullet$ which may consume the reactive sites of PE backbone and decrease the possibility of crosslinking [reactions (3), (4), (5), (6)].

The reactions (1) and (3) will occur simultaneously according to the Process 3 in Fig. 4-15. It means that the crosslinking reaction [reaction (2)] and the grafting reactions [reactions (4), (5), and (6)] will compete with each other. Thus, the crosslinking degree of process 3 will be larger than that of process 1 and smaller than that of process 2. In Table 4-4, all cases are processed according to Process 1, little crosslinking is obtained at various reaction conditions and compositions. Therefore, it is obvious that the process 1 has the lowest gel content.
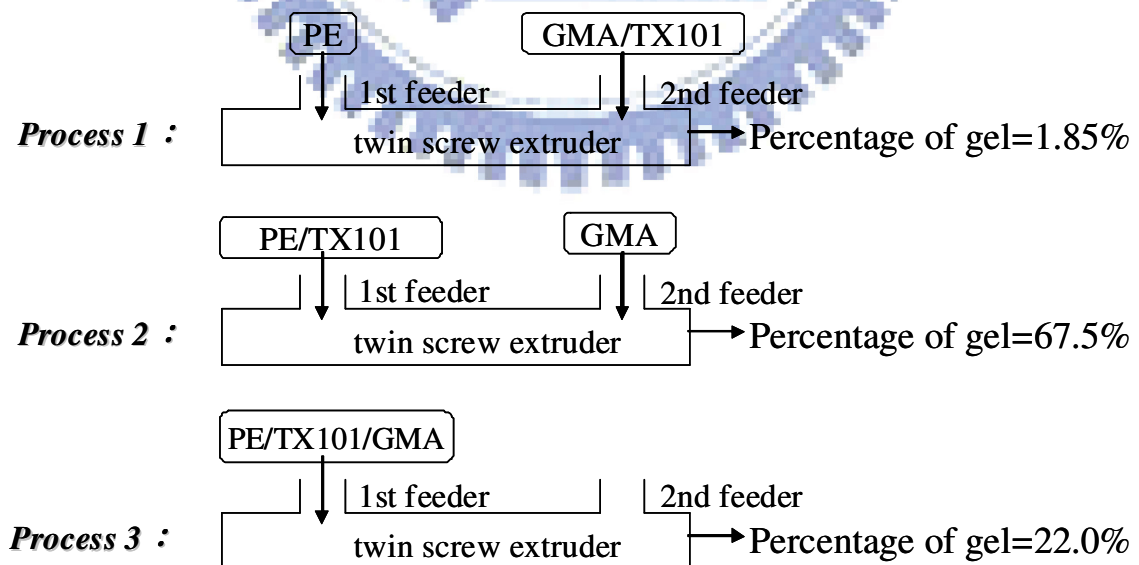
Fig. 4-15.The Different Types of Grafting Procedure

4.5.3. Estimation of the Percentage of Grafting for Compatibilizers

FTIR spectra of pure LDPE and PE-g-GMA are presented in Figs. 4-16(a) and 4-16(b), respectively. As shown in Fig. 4-15 (b), the absorption bands at 846, 908, and 995 cm^{-1} are the characteristic vibrations of epoxy groups [45], indicating the occurrence of grafting reaction (Scheme 3-3). As to the percentage of grafting (%grafting), it can be directly calculated by the ratio of the absorbance of the carbonyl group for PE-g-GMA to that of the methylene group for pure LDPE. However, this method is tedious. In order to simplify the determination of %grafting, we draw the calibration curve [46] in terms of the experimental results of extrudates **a**, **b**, **c**, and **d** (Table 4-4) as shown in Fig. 4-17, whose abscissa is the ratio of carbonyl stretch (νCO, 1731 cm^{-1}) to the methyl stretch (δCH_3, 1376 cm^{-1}) for PE-g-GMA (*i.e.*, $\nu CO/\delta CH_3$) and ordinate is the content of oxygen for PE-g-GMA (%oxygen), respectively. The $\nu CO/\delta CH_3$ and %oxygen are measured by FTIR and element analysis, respectively.
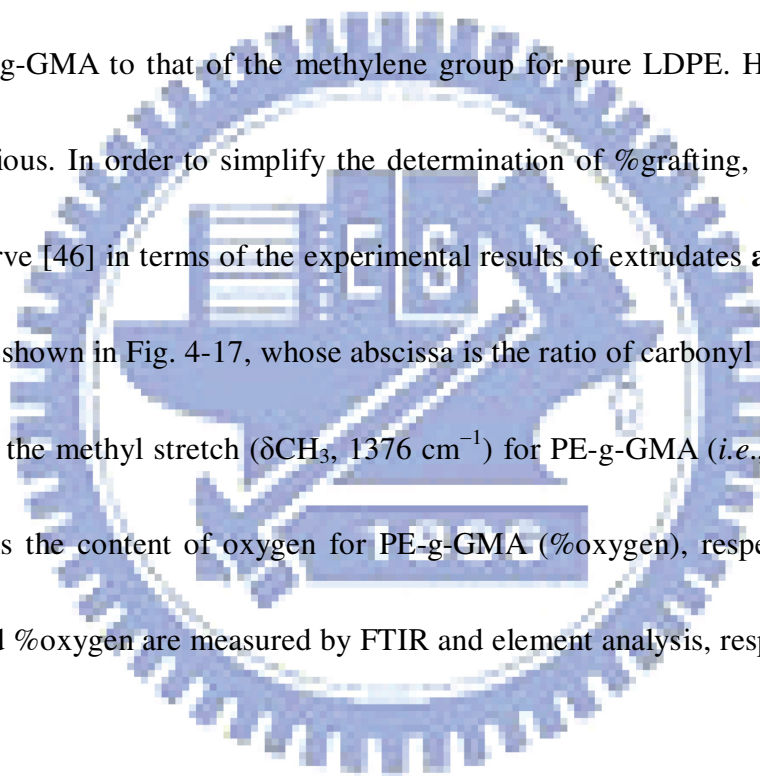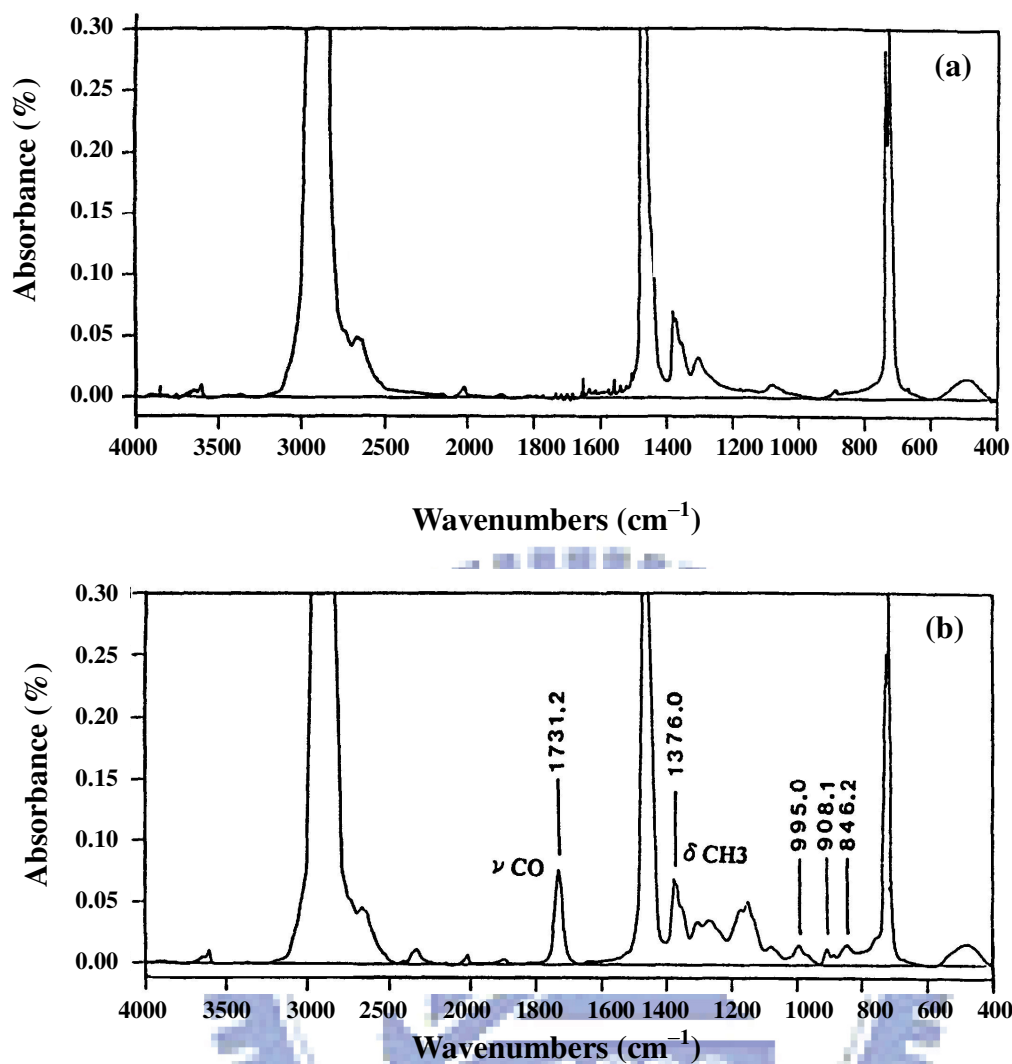
Fig. 4-16. FTIR spectra of (a) pure LDPE and (b) PE-g-GMA.

Since the linear calibration curve has been successfully established, the %grafting can be rapidly estimated from the %oxygen as shown in Fig. 4-17, whose acquirement is much easier than $\nu CO/\delta CH_3$, through fitting of the linear calibration curve. For example, in case of extrudates **e,** we obtain %oxygen (0.16) from the FTIR result and then the %grafting can be determined to be 0.48 by matching the calibration curve (Fig. 4-16).

Table 4-4. Summary of the experimental results of grafting reactions.

Extrudate	Composition of LDPE/GMA/TX101 (*wt./wt./wt.*)	Screw speed (rpm)	Processing temp.(°C)	$\nu CO/\delta CH_3$	%oxygen	%grafting	%gel
a	100/40/0.2	100	120	2.49	1.42	4.20	-
b	100/20/0.8	200	200	2.44	1.45	4.29	-
c	100/30/1	300	220	2.98	1.75	5.18	-
d	100/5/2	100	275	0.96	0.60	1.78	-
e	100/10/0.27	200	220	---	0.16	0.48	0.43
f	100/10/0.53	200	220	---	0.21	0.62	0
g	100/10/0.80	200	220	---	0.28	0.82	0
h	100/10/0.53	300	220	---	0.11	0.33	0
i	100/10/0.53	100	220	---	0.26	0.77	0
j	100/15/0.27	200	220	---	0.20	0.59	0
k	100/15/0.27	200	145	---	0.05	0.14	0
l	100/15/0.27	200	255	---	0.58	1.72	0.3
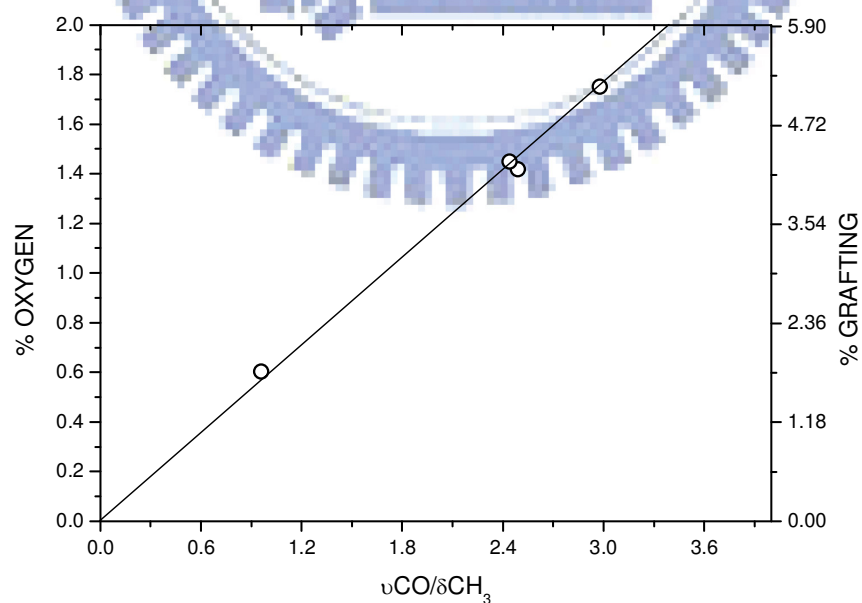
Fig. 4-17. The calibration curve for PE-g-GMA.

4.5.4. Dependence of Processing Parameters on Grafting Reaction of Extrusion for Compatibilizers

As shown in Table 4-4, the %grafting is strongly dependent on the processing parameters such as concentration of initiator, screw speed, concentration of GMA, and processing temperature. In case of the extrudates **e**, **f**, and **g**, %grafting increases with the rising of concentration of initiator (TX 101), revealing higher concentration of TX 101 promotes the initiation of grafting reaction (reaction (1) of Fig. 4-14) and raises the %grafting. Furthermore, a comparison of the experimental results of extrudates **f**, **h**, and **i** indicates the %grafting decreases with the increase of screw speed, revealing the faster screw speed shortens the residence time of reactants in the extruder and thus reduces the %grafting. In case of extrudates **e** and **j**, %grafting rises with the raising of concentration of reactant (GMA). In addition, it was also found that the processing temperature highly influences the %grafting. As shown in the experimental results of extrudates **j**, **k**, and **l**, the %grafting heightens with the increase of the processing temperature; manifesting higher temperature causes higher speed and yield of grafting reaction. Therefore, we can ingeniously manipulate the %grafting by the modulation of processing parameters. In the near future, we will keep on analyzing the influence of the grafting procedure on grafting efficiency by statistical methods to acquire more detailed results.

4.5.5. Thermal Properties of PE-g-GMA Compatibilizers

PPS alloys have been produced before with appropriate commercially available compatibilizers (*e.g.*, PE-g-acrylic acid, PE-g-maleic anhydride, *etc*.) [46-49]. However, these compatibilizers exhibit poor thermal stability, limiting the applications of PPS alloys. Fig. 4-18 illustrates the TGA curve of PE-g-GMA. In case of PE-g-GMA, no degradation occurred until 300°C in nitrogen ambient and its decomposition temperature could reach 372°C. In comparison with the commercially available compatibilizer (PE-g-acrylic acid), PE-g-GMA apparently exhibits a superior thermal stability since the epoxy group in PE-g-GMA can be more effective in resisting the heat than the carboxyl acid group of PE-g-acrylic acid. This result reveals that PE-g-GMA is a better compatibilizer for alloys of high performance engineering plastics, *e.g.*, PPS/PET or PPS/nylon 66, *etc*., than PE-g-acrylic acid.
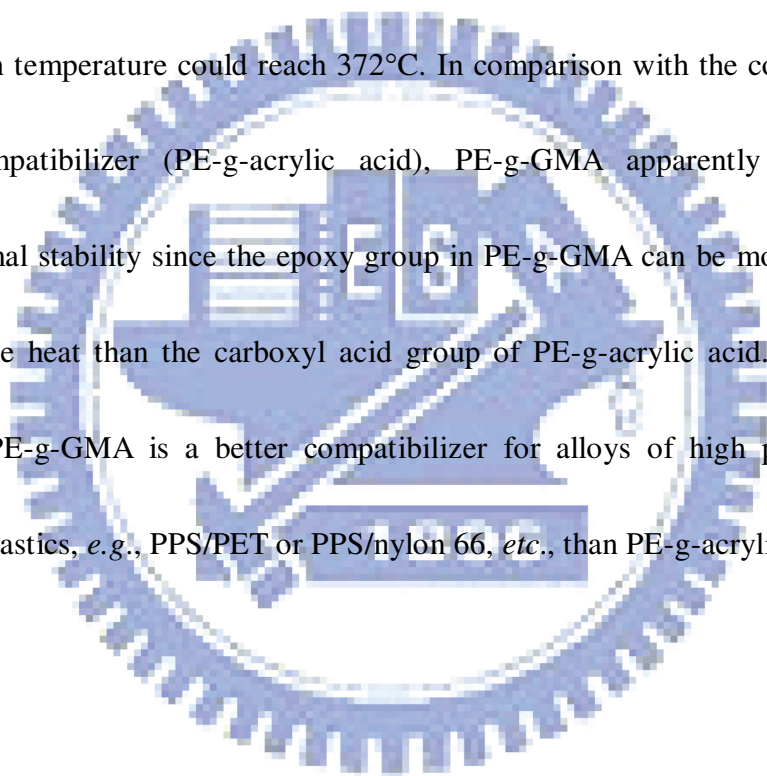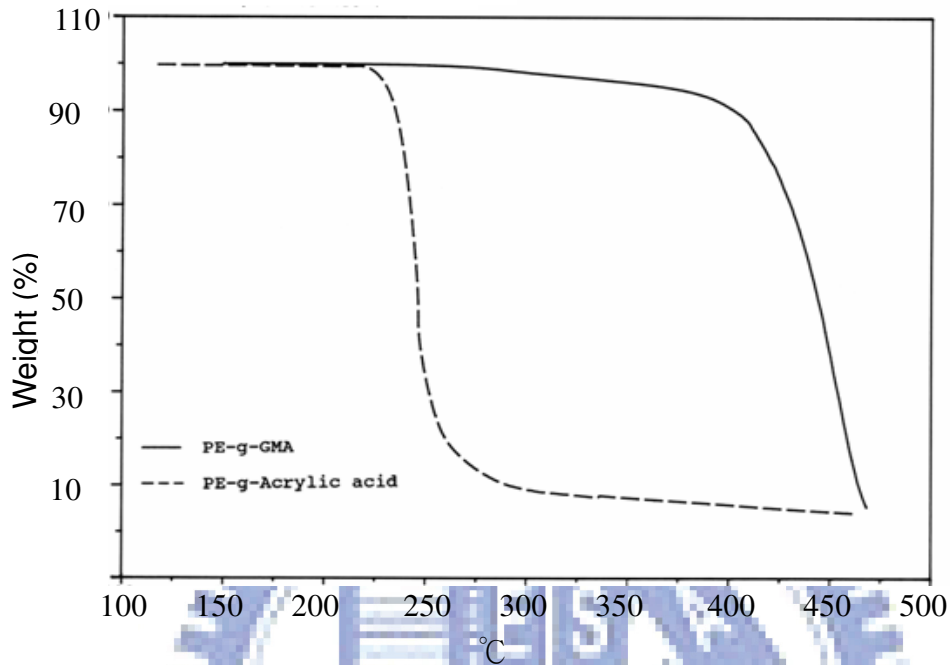
Fig. 4-18. TGA curves of PE-g-GMA and PE-g-acrylic acid in nitrogen ambient.

4.5.6. PE-g-GMA as a Compatibilizer of PPS/PET and PPS/nylon 6,6/glass Fiber

Alloys

The PPS, PET and PE-g-GMA were blended in the twin screw extruder and the

specimens for subsequent tests were prepared by injection molding. The blend

compositions and the mechanical properties of the PPS/PET alloys are tabulated in

Table 4-5. The experimental results illustrate that the unnotched impact strength of

PPS/PET alloys with PE-g-GMA (alloy **n**) is higher than that without PE-g-GMA

(alloy **m**), indicating the introduction of PE-g-GMA is capable of promoting the

mechanical properties. Furthermore, the improvement of compatibility for PPS/PET alloys could be deduced from the results of SEM observation. As shown in Fig. 4-19(a), alloy **m** exhibits the morphology with an incompatible phenomenon, while alloy **n** (Fig. 4-19(b)) exhibits the morphology with fine and uniform dispersion, manifesting the enhancement of the compatibility between PPS and PET by PE-g-GMA since the epoxy group of PE-g-GMA may attract with the carboxyl as well as oxygen groups of PET and the sulfide group of PPS *via* strong van der Waal forces.

Table 4-5. Summary of the experimental results of PPS/PET alloys.

Alloy	Composition of PPS/PET/PE-g-GMA (*wt.*/*wt.*/*wt.*)	*Unnotched impact strength (kg.cm/cm)
m	100/50/0	6.81
n	100/50/12.5	10.0

*measured at 25°C after aging at 240°C for 231 hrs (the standard deviations = ±2%).

In order to further raise the mechanical properties of PPS, we also introduced nylon 6,6 and glass fiber into the PPS to form PPS/nylon 6,6/glass fiber alloys *via* the same procedures described above. As shown in Table 4-6, the PE-g-GMA is an excellent compatibilizer of PPS/nylon 6,6/glass fiber alloys since the impact strength
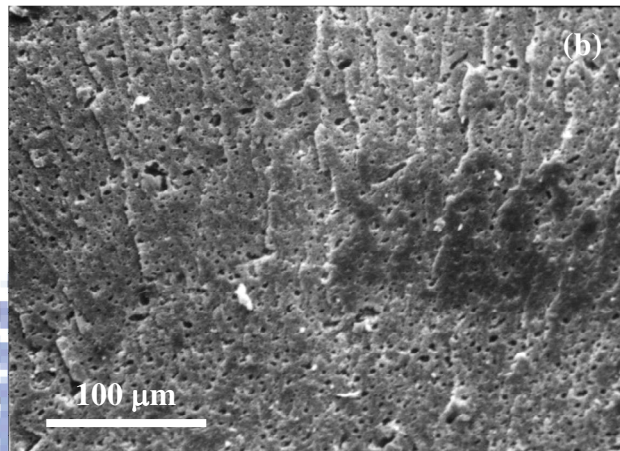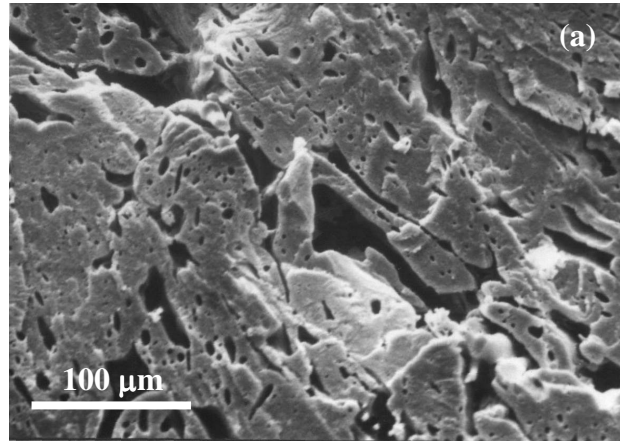
Fig. 4-19. SEM micrographs of PPS/PET alloys (a) without PE-g-GMA (b) with the

PE-g-GMA.

of alloy **p** is higher than alloy **o** due to the generation of strong van der Waal forces in

between the epoxy group of PE-g-GMA and the amine group of nylon 6,6 as well as

the sulfide group of PPS. Moreover, chemical reaction between the nylon 6,6 and the

PE-g-GMA may proceed from the amine addition [10], further promoting the

compatibility of PPS/PA6,6 alloys. As shown in Tables 4-5 and 4-6, in addition, the

impact strength of PPS/nylon 6,6/glass fiber alloys with PE-g-GMA (alloy **p**) is much

higher than that of PPS/PET alloys with PE-g-GMA (alloy **n**), revealing that addition

of nylon 6,6 and glass fiber can drastically increase the mechanical properties of PPS.

Table 4-6. Summary of the experimental results of PPS/nylon 6,6/glass fiber
alloys.

Alloy	Composition of PPS/nylon 6,6/glass fiber/PE-g-GMA (*wt./wt./wt./wt.*)	*Unnotched impact strength (kg.cm/cm)
o	100/50/45/0	78
p	100/50/45/12.5	>100

*measured at 25°C after aging at 240°C for 231 hrs (the standard deviations = ±2%).

4.5.7. Physical Properties of the Reflector Cups for LEDs

As shown in Fig. 4-20 and Table 4-7, the reflector cups for LEDs exhibit excellent

mechanical properties (yield strength = 650 kg/cm^2; modulus of elasticity = 24,500

kg/cm^2), outstanding thermal resistance (heat deflection temperature = 245°C;

IR-reflow = 260°C), good inflammability (UL94-V-0) and high reflectance (90 – 95%),

meeting the preliminary requirements.
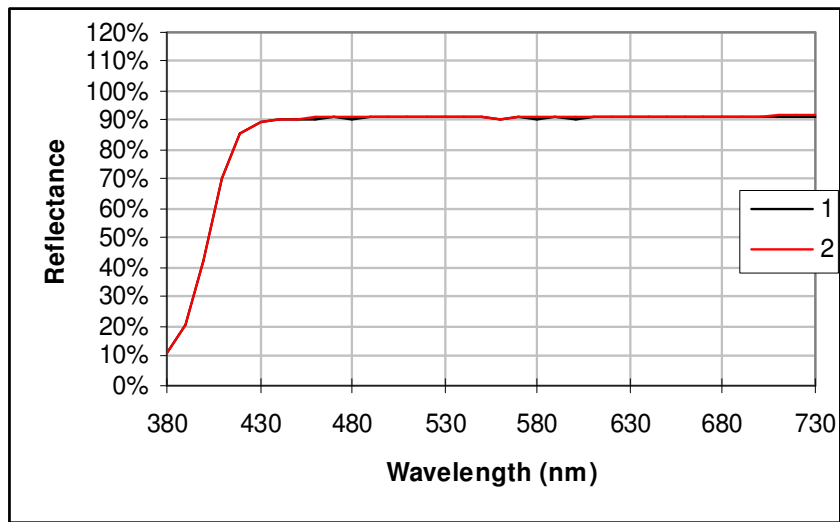
Fig. 4-20. Reflectance of the reflector cups for LEDs.

Table 4-7. Physical Properties of the reflector cups for LEDs.

Test item	Test result	Test standard
Yield strength	650 kg/cm^2	ASTM D790
Modulus of elasticity	24500 kg/cm^2	ASTM D790
Impact strength	1.0 ft-lb/in of notched	ASTM D256
Heat distortion temperature	245°C	ASTM D648
IR-Reflow	260°C	
Reflectance	90 - 95%	
Inflammability	V-0	UL94-V

4.5.8. Encapsulation of LEDs with Silicone-acrylate Nanocomposite

The physical properties of silicone-acrylate nanocomposite not only affect the

lifetimes of LEDs but also their extract efficiencies. As shown in Eq. (4-1), the extract

efficiencies ($\eta_{extract}$) of LEDs are dependent on the refractive indices of blue chip (n_{chip})

and silicone-acrylate nanocomposite (n_{gel}).

$$\eta_{extract} = 1 - \eta_{whole\ reflection} = 1 - \frac{\left(n_{chip} - n_{gel}\right)^2}{\left(n_{chip} + n_{gel}\right)^2} = \frac{4n_{chip}n_{gel}}{\left(n_{chip} + n_{gel}\right)^2} \qquad (4\text{-}1)$$

where $\eta_{whole\ reflection}$ represent the extract and whole reflection efficiencies.

Because $n_{chip} = 3.6$, Eq. (4-1) can be thus be rewritten as

$$\eta_{extract} = \frac{14.4n_{gel}}{\left(3.6 + n_{gel}\right)^2} \qquad (4\text{-}2)$$

With Eq. (4-2), the extract efficiencies of LEDs without encapsulation and with

encapsulation of silicone-acrylate nanocomposite can be calculated to be 0.69 and 0.83,

respectively, since the refractive indices of air and silicone-acrylate nanocomposite are

1.05 and 1.48, respectively.

When the LED is actuated at 3 V, the luminance of LEDs without encapsulation

abruptly slumps from 3,300 cd/m^2 and their half-lifetimes, defined as the duration while

the luminance decays from the original amount to its half, are 2,400 hrs as shown in Fig.

4-21. With encapsulation of silicone-acrylate nanocomposite, however, the luminance

and half-lifetimes of LEDs increase to 4,900 cd/m^2 and 18,300 hrs, respectively, due to

the high extract efficiencies (0.83) and excellent gas barrier capabilities. In comparison

with commercial UV-curable encapsulating adhesives for LEDs (EPO-TEK H20S;

Epoxy technology Inc.), whose refractive indices and extract efficiencies are 1.45 and

0.81, respectively, silicone-acrylate nanocomposite exhibits faster curing duration,

longer lifetimes, and higher original luminance as shown in Fig. 4-21 in comparison

with the curing duration, half-lifetimes, and original luminance of LEDs with

EPO-TEK H20S are 10 min, 9,500 hrs, and 4,400 cd/m^2, respectively.
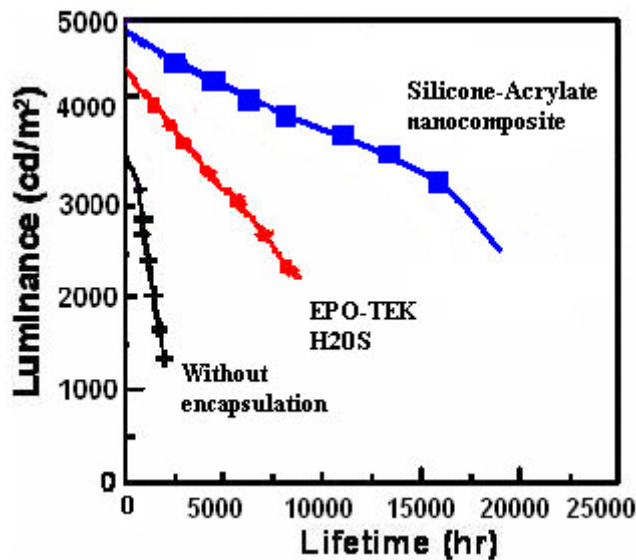
Fig. 4-21. Lifetimes of LED sample without encapsulation and encapsulation with

various resins.

Chapter 5

Conclusions

We have successfully increased the lifetimes of OLEDs by the introduction of protection layer (LiF) and encapsulating adhesives (PU-Acrylate), which can be synthesized by swift UV procedure. With LiF and encapsulating adhesives, the half-lifetimes of devices can be heightened to 18 times longer than those without encapsulation.

By the manipulation of NPB/ADS082BE layer thickness and addition of electron blocking layer, we have also successfully manufactured color/luminance tunable OLEDs with high electroluminescent intensity and low turn-on voltage. Moreover, the lifetimes of lab-made OLEDs and LEDs with encapsulation of Silicone-Acrylate have been promoted to be approximately 11 and 7.6 folds longer than those without encapsulation.

Novel UV curable organic/inorganic hybrid nanocomposites (Epoxy-Acrylate/silica/Invar) with excellent gas barrier performance, moderate adhesion strength, low shrinkage, good thermal resistance, and fast curing speed have been successfully synthesized and applied for the encapsulation of organic solar cells. We have found that lab-made nanocomposites effectively impede the penetration of

moisture and oxygen in the atmosphere into the device and consequently prolong the lifetimes of organic solar cells.

In addition, fabrication of polymeric reflector cups for LEDs by using polyphenylene sulfide/poly(ethylene terephthalate) (PPS/PET) and PPS/nylon 6,6/glass fiber alloys *via* injection molding process are also presented in this work. Grafting extrusion of epoxy-modified polyethylene (PE-g-GMA) was successfully performed and the percentage of grafting could be rapidly estimated by the linear calibration curve. With PE-g-GMA as a compatibilizer, PPS/PET and PPS/nylon 6,6/glass fiber alloys are homogenously dispersed and their unnotched impact strengths were effectively promoted due to strong van der Waal forces between the epoxy group of PE-g-GMA and functional groups of polymers.
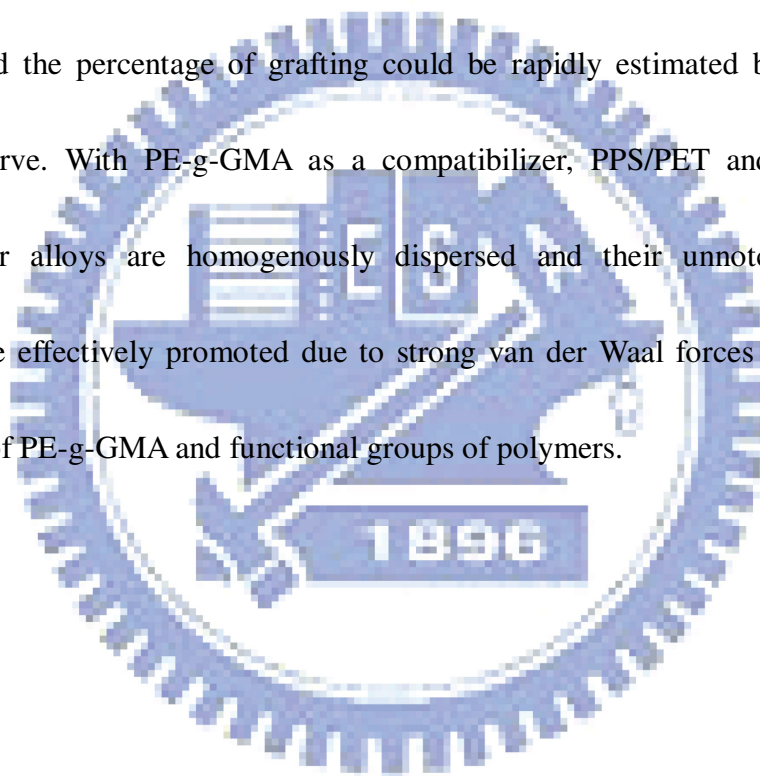
Prospective Researches

In the near future, we will introduce other functional groups (*e.g*., epoxy, urethane, silicone, amine, etc.) into the acrylate backbone with appropriate prescription of photoinitiators and fillers to further promote the physical properties (e.g. adhesive strength, gas penetration, and transparency, *etc*.), meeting the requirements of gas barrier materials for commercial photoelectric devices. Furthermore, faster and more effective synthesizing procedure (e.g. microwave, etc.) and coating process (e.g. screen printing, etc.) will also be utilized for the preparation of encapsulating materials and package of photoelectric devices, respectively.
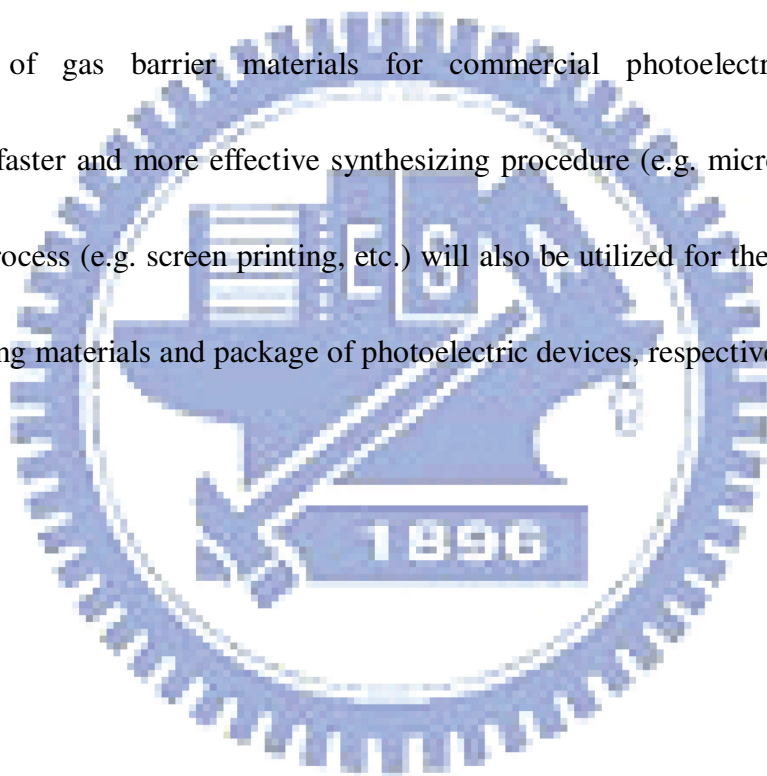
References

[1] K. Zeng and Y.P. Bai, "Improve the gas barrier property of PET film with montmorillonite by in situ interlayer polymerization", *Mater. Lett.*, **59**(2005), p.3348.

[2] K. Müllen and U. Scherf, *Organic Light Emitting Devices: Synthesis, Properties and Application*, Wiley-VCH, New York, (2006), p.410.

[3] A. Bettencourt-Dias, "Lanthanide-based emitting materials in light-emitting diodes", *Dalton Trans.*, **22**(2007), p.2229.

[4] C.H. Chen and J. Shi, "Metal chelates as emitting materials for organic electroluminescence", *Coordination Chemistry Reviews*, 171(1998), p.161.

[5] S. Wang, "Luminescence and electroluminescence of Al(III), B(III), Be(II) and Zn(II) complexes with nitrogen donors", *Coordination Chemistry Reviews*, **215**(2001), p.79.

[6] H. Meng and Z.R. Li, *Organic Light-emitting Materials and Devices*, RSC Press, London, 2006, p.672.

[7] S.F. Lim, W. Wang and S.J. Chua, "Degradation of organic light-emitting devices due to formation and growth of dark spots", *Mat. Sci. Eng. B*, **85**(2001), p.154.

[8] L.M. Do, K. Kim, T. Zyung, H.K. Shim and J.J. Kim, "In situ investigation of degradation in polymeric electroluminescent devices using time-resolved confocal

laser scanning micorscope", *Appl. Phys. Lett.*, **70**(1997), p.3470.

[9] T.H. Chiang, "A Study and Property Modification of UV-curable Epoxide Resins Applied to OLED Packaging", *Ph.D. Thesis of National Chiao Tung Univeristy*, (2006), p.7.

[10] A.V. Pocius, *Adhesion and Adhesive Technology: an Introduction*. New York: Munich/Hauser publishers, (1997), p.215.

[11] C. Decker, L. Keller, K. Zahouily and S. Benfarhi, "Synthesis of nanocomposite polymers by UV-radiation curing", *Polymer,* **46**(2005), p.6640.

[12] F. Bauer, R. Flyunt, K. Czihal, H. Langguth, R. Mehnert, R. Schubert and M.R. Buchmeiser, "UV curing and matting of acrylate coatings reinforced by nano-silica and micro-corundum particles", *Prog in Org. Coatings*, **60**(2007), p.121.

[13] G. Malucelli, R. Bongiovanni, M. Sangermano, S. Ronchetti and A. Priola, "Preparation and characterization of UV-cured epoxy nanocomposites based on *o*-montmorillonite modified with maleinized liquid polybutadienes", *Polymer*, **48**(2007) p.7000.

[14] C.W. Tang and S.A. Van Slyke, "Organic electroluminescent diodes", *Appl. Phys. Lett.*, **51**(1987), p.913.

[15] A.N. Krasnov, "High-contrast organic light-emitting diodes on flexible substrates", *Appl. Phys. Lett.*, **80**(2002), p.3853.

[16] J. Shi and C.W. Tang, "Anthracene derivatives for stable blue-emitting organic electroluminescence devices", *Appl. Phys. Lett.*, **80**(2002), p.3201.

[17] Y. Leterrier, "Durability of nanosized oxygen-barrier coatings on polymers - Internal stresses", *Prog. in Mater. Sci.*, **48**(2003), p.1.

[18] K. Yamashita, T. Mori and T. Mizutani, "Encapsulation of organic light-emitting diode using thermal chemical-vapour-deposition polymer film", *J. Phys. D. Appl. Phys.*, **34**(2001), p.740.

[19] H. Kanno, Y. Hamada and H. Takahashi, "Development of OLED with high stability and luminance efficiency by co-doping methods for full color displays", *IEEE J. Selec. Topics Quantum Electron.*, **10**(2004), p.30.

[20] H. Kim, W.W. So and S. J. Moon, "The importance of post-annealing process in the device performance of poly(3-hexylthiophene): Methanofullerene polymer solar cell", *Solar Energy Materials and Solar Cells*, **91**(2007), p.581.

[21] J. Guo, G. Yu and A. J. Heeger, "Polymer p-i-n junction photovoltaic cells", *Advanced Materials*, **10** (1998) p.692.

[22] S.E. Shaheen, C.J. Brabec, N.S. Sariciftci, F. Padinger, T. Fromherz and J.C. Hummelen, "2.5% efficient organic plastic solar cells", *Appl. Phys. Lett.*, **78**(2001), p.841.

[23] G. Li, V. Shrotriya, J. Huang, Y. Yao, T. Moriarty, K. Emery and Y. Yang, "High-efficiency solution processable polymer photovoltaic cells by self-organization of polymer blends", *Nature Materials*, **4**(2005), p.864.

[24] W. Ma, C. Yang, X. Goung, K. Lee and A.J. Hegger, "Thermally stable, efficient polymer solar cells with nanoscale control of the interpenetrating network morphology", *Adv. Funct. Mate*r., **15**(2005), p1617.

[25] M. Al-Ibrahima, H.-Klaus Roth, U. Zhokhavets, G. Gobsch and S. Sensfuss, "Flexible large area polymer solar cells based on poly(3-hexylthiophene)/fullerene", *Sol. Energ. Mat. Sol. C.*, **85**(2005), p.13.

[26] S.H. Jin, B.V.K. Naidu, H.S. Jeon, S.M. Park, J.S. Park, S.C. Kim, J.W. Lee and Y.S. Gal, "Optimization of process parameters for high-efficiency polymer photovoltaic devices based on P3HT:PCBM system", *Sol. Energ. Mat. Sol. C.*, **91**(2007), p.1187.

[27] S.K. Kim, B.H. Hwang, J.H. Lee, J.I. Kang, K.W. Min and W.Y. King, "2.4-in. monochrome small molecular OLED display for mobile application", *Curr. Appl. Phys.*, **2** (2002) 335.

[28] B.M. Henry, F. Dinelli, K.Y. Zhao, C.R.M. Grovenor, O.V. Kolosov, G.A.D. Briggs, A.P. Roberts, R.S. Kumar and R.P. Howson, "A microstructural study of transparent metal oxide gas barrier films", *Thin Solid Films*, **355**(1999), p.500.

[29] E.M. Moser, R. Urech, E. Hack, H. Kuenzli and E. Mueller, "Hydrocarbon films inhibit oxygen permeation through plastic packaging material", *Thin Solid Films*, **317**(1998), p.388.

[30] A.G. Erlat, B.M. Henry, J.J. Ingram, D.B. Mountain, A. McGuigan, R.P. Howson, C.R.M. Grovenor, G.A.D. Griggs and Y. Tsukahara, "Characterisation of aluminium oxynitride gas barrier films", *Thin Solid Films*, **388**(2001), p.78.

[31] G.H. Kim, J. Oh, Y.S. Yang, L.M. Do and K.S. Suh, "Encapsulation of organic light-emitting devices by means of photopolymerized polyacrylate films", *Polymer*, **45**(2004), p.1879.

[32] Y.S. Jeong, B. Ratier, A. Moliton and L. Guyard, "UV–visible and infrared characterization of poly(*p*-xylylene) films for waveguide applications and OLED encapsulation", *Synthetic Met.*, **127**(2002), p.189.

[33] C. Charton, N. Schiller, M. Fahland, A. Hollander, A. Wedel and K. Noller, "Development of high barrier films on flexible polymer substrates", *Thin Solid Films*, **502**(2006), p.99.

[34] M. Alexandre and P. Dubois, "Polymer-layered silicate nanocomposites: preparation, properties and uses of a new class of materials", *Mater Sci Eng R.*, **28**(2000), p.1.

[35] S. Takahashi, H.A.Goldberg, C.A. Feeney, D.P. Karim, M. Farrell, K. O'Leary and D.R. Paul DR, "Gas barrier properties of butyl rubber/vermiculite nanocomposite coatings", *Polymer*, **47**(2006), p.3083.

[36] M. Frounchi, S. Dadbin, Z. Salepour and M. Noferesti, "Gas barrier properties of PP/EPDM blend nanocomposites", *J. Mem. Sci.*, **282**(2006), p.142.

[37] T. Ogasawara, Y. Ishida, T. Ishikawa, T. Aoki and T. Ogura, "Helium gas permeability of montmorillonite/epoxy nanocomposites", *Composites, Part A*, **37**(2006), p.2236.

[38] E. Picard, A. Vermogen, J.F. Gerard and E. Espuche, "Barrier properties of nylon 6-montmorillonite nanocomposite membranes prepared by melt blending: Influence of the clay content and dispersion state: Consequences on modelling", *J. Mem. Sci.*, **292**(2007), p.133.

[39] K. Yano, A. Usuki, A. Okada, T. Kurauchi and O. Kamigatio, "Synthesis and properties of polyimide-clay hybrid," *J. Polym. Sci. A: Polym. Chem.*, **31**(1993), p.2493.

[40] Y.Y. Wang, "Preparation and Property Characterizations of UV-curable

Nano-composite Sealing Resins for OLED Packaging", *Ph.D. Thesis of National Chiao Tung Univeristy*, (2007), p.32.

[41] J.T. Lutz, Jr. and R. F. Grossman, *Polymer Modifiers and Additives*, Marcel Dekker, New York, (1988), p.260.

[42] S.J. Lin, H.Y. Ueng and F.S. Juang, ": Effects of thickness of organic and multilayer anode on luminance efficiency in top-emission organic light emitting diodes", *Jpn. J. of Appl. Phys.*, **45**(2006), p.3717.

[43] F.X. Zang, T.C. Sum, A.C.H. Huan, T.L. Li, W.L. Li and F. Zhu, "Reduced efficiency roll-off in phosphorescent organic light emitting diodes at ultrahigh current densities by suppression of triplet-polaron quenching", *Appl. Phys. Lett.*, **93**(2008), p.023309-1.

[44] R.R. Gallucci and R.C. Going, "Preparation and reactions of epoxy-modified polyethylene", *J. Appl. Polym. Sci.*, **2**7(1982), p.425.

[45] K. Nakanishi, *Infrared Absorption Spectroscopy*, Holden-Day, San Francisco, (1962), p.58.

[46] J.G. Martinez, R. Benavides, C. Guerrero and B.E. Reyes, "UV sensitisation of polyethylenes for grafting of maleic anhydride", *Polymer Degradation and Stability*, **86**(2004), p.129.

[47] T. Hisamatsu, S. Nakano, T. Adachi, M. Ishikawa and K. Iwakura, "The effect of

compatibility on toughness of PPS/SEBS polymer alloy", *Polymer*, **41**(2000),

p.4803.

[48] F.P. Tseng, J.J Lin, C.R. Tseng and F.C. Chang, "Poly(oxypropylene)-amide

grafted polypropylene as novel compatibilizer for PP and PA6 blends", *Polymer*,

42(2001), p.713.

[49] N.C. Liu, H.Q. Xie and W.E. Baker, "Comparison of the effectiveness of different

basic functional groups for the reactive compatibilization of polymer blends", *Polymer*,

34(1993), p.4680.

Curriculum Vitae

Chen-Ming Chen (陳建明)

PERSONAL DATA

Born: Oct. 3, 1965, Taoyuan, Taiwan

Nationality: Taiwan, Republic of China

Office Address: Department of Materials Science and Engineering, National Chiao-Tung University, Hsinchu, Taiwan 30010, ROC.

Tel: +886-3-5712121-55338

E-mail: JeremyChen@itri.org.tw

EDUCATION

Ph.D. candidate, Department of Materials Science and Engineering, National Chiao-Tung University, Hsinchu, Taiwan, present.

Master of Engineering, Department of Chemical Engineering, National Central University, Taiwan, July (1990)

Bachelor of Engineering, Department of Chemical Engineering, Chung Yuan Christan University, Taiwan, July (1988)

PUBLICATIONS

Journal articles

1. **Chen-Ming Chen**, Tsung-Eong Hsieh, and Mark O. Liu, "Preparation of epoxy-modified polyethylene by graft extrusion and its applications to polyphenylene sulfide alloys as a compatibilizer", *Reactive and Functional*

Polymers 68 (2008) 1307-1313.

2. **Chen-Ming Chen**, Ming-Hua Chung,Tsung-Eong Hsieh, Mark O. Liu, Jen-Lien Lin, Wei-Ping Chu, Rong-Ming Tang, Yu-Sheng Tsai and Fuh-Shyang Juang, "Synthesis, thermal characterization, and gas barrier properties of UV curable organic/inorganic hybrid nanocomposites with metal alloys and their application for encapsulation of organic solar cells", *Composites Science and Technology* 68 (2008) 3041-3046.

3. **Chen-Ming Chen**, Ming-Hua Chung, Tsung-Eong Hsieh, Bohr-Ran Huang, Huai-En Hsieh, Fuh-Shyang Juang, Yu-Sheng Tsai, Mark O. Liu, and Jen-Lien Lin, "Electroluminescent properties of color/luminance tunable organic light emitting diodes and their lifetime enhancement with encapsulation", *Materials Science and Engineering B* 153 (2008) 100-105.

4. **Chen-Ming Chen**, Ming-Hua Chung, Tsung-Eong Hsieh, Bohr-Ran Huang, Huai-En Hsieh, Fuh-Shyang Juang, Yu-Sheng Tsai, Mark O. Liu, and Jen-Lien Lin, "Ultraviolet-assisted synthesis of encapsulating adhesives and their application for lifetime improvement of organic light emitting diodes", *Current Applied Physics* 9 (2009) 746-749.

5. Ming-Hua Chung, **Chen-Ming Chen**, Tsung-Eong Hsieh, Rong-Ming Tang, Yu Sheng Tsai, Wei-Ping Chu, Mark O. Liu, and Fuh-Shyang Juang, "Comparison of the use of different encapsulating adhesives to enhance the efficiencies and lifetimes of polymeric solar cells", *Japanese Journal of Applied Physics* 48 (2009) 04C177.

6. **Chen-Ming Chen**, Tsung-Eong Hsieh and Ming-Yih Ju, "Effects of Polydispersity Index and Molecular Weight on Crystallization Kinetics of Syndiotactic Polystyrene (sPS)", *J. Alloy Compd.*, (2009), in press.

Conference papers

1. **<u>Chien-Ming Chen</u>**, Ming-Hua Chang, Tsung-Eong Hsieh, Rong-Ming Tang, Yu Sheng Tsai, Wei-Ping Chu, Mark O. Liu, and Fuh-Shyang Juang, "Comparison of the use of different encapsulate adhesion glue to enhance the efficiency and lifetime of polymer solar cells", *International Conference on Solid State Devices and Materials, Tsukuba Ibaraki*, Japan, Sep, 23-26, 2008.